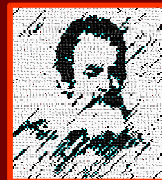


Open Issues in Cosmology

Sabino Matarrese

Dipartimento di Fisica “*Galileo Galilei*”
Università degli Studi di Padova

INFN, Sezione di Padova



We have a standard model of cosmology

- General Relativity + Uniform Universe [Big Bang]
Density and ingredients of the universe determines its fate
- 2. Universe is essentially flat (total density = critical density)
 1. Atoms 4%
 2. Dark Matter 23%
 3. Dark Energy (*cosmological constant?*) 72%
- 3. Universe has tiny ripples which were originated during Inflation
 1. *Adiabatic, scale-invariant, quasi-Gaussian fluctuations*
 2. *Gravitational wave background (still to be detected)*

We have entered the “Era of Precision Cosmology”

Very large datasets will soon become available in Cosmology:

*Large galaxy redshift surveys (2dF, SDSS, ...) allow to study the Large-Scale Structure (**LSS**) of the Universe*

*Present and ongoing satellite missions like WMAP and Planck allow to measure the temperature anisotropy and polarization of the Cosmic Microwave Background (**CMB**) radiation with unprecedented precision*

*The **SNAP** satellite will collect redshifts for a large number of high-redshift type Ia Supernovae (**SN**)*

Open issues (March 2006)

Understanding the nature of DM

Understanding the nature of DE

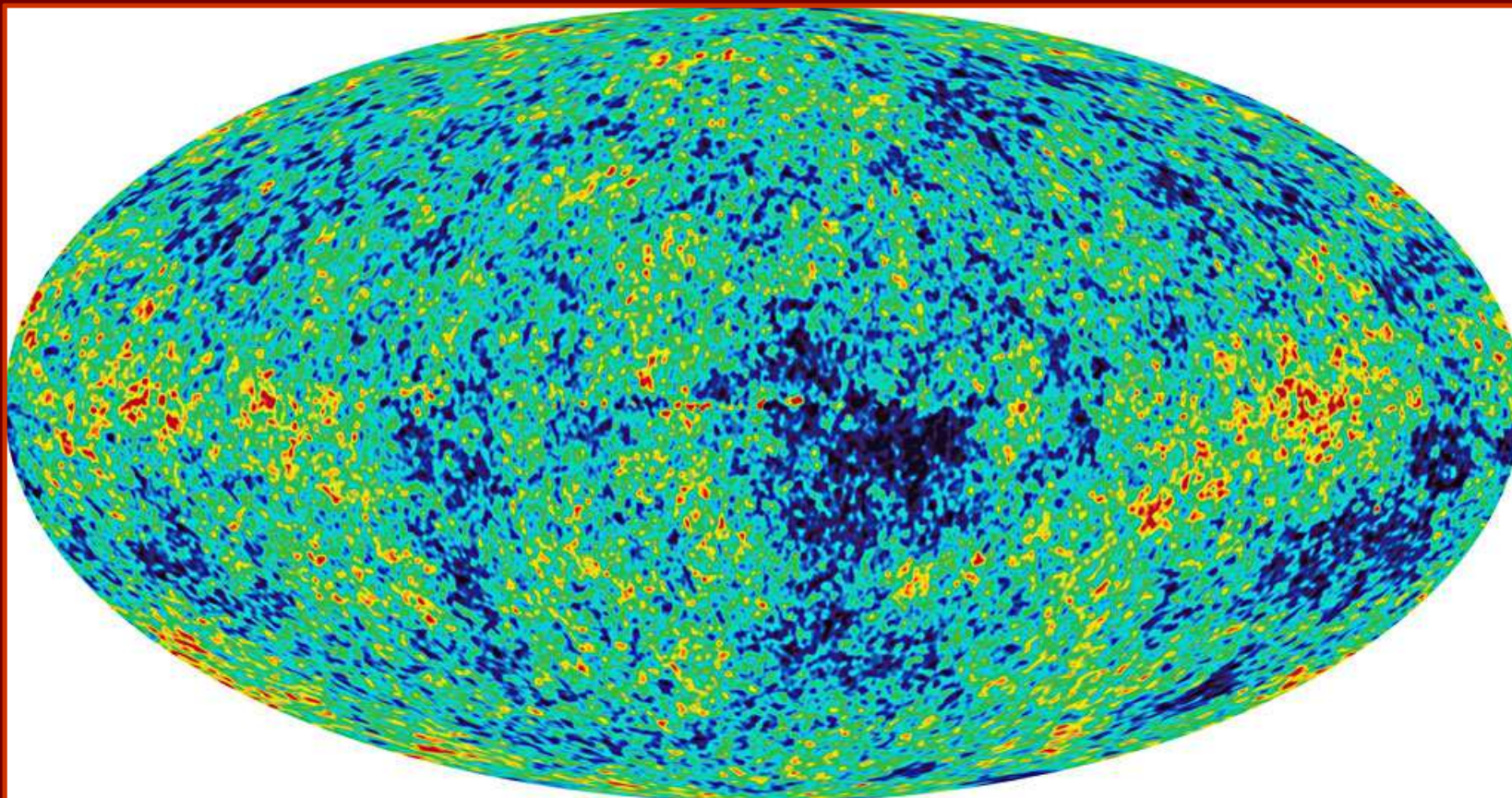
Solving the DM-DE coincidence problem

Falsifying the inflationary paradigm

Detecting the primordial GW background

Understanding the origin of cosmic magnetic
fields

The microwave sky as seen by WMAP



WMAP anisotropy data

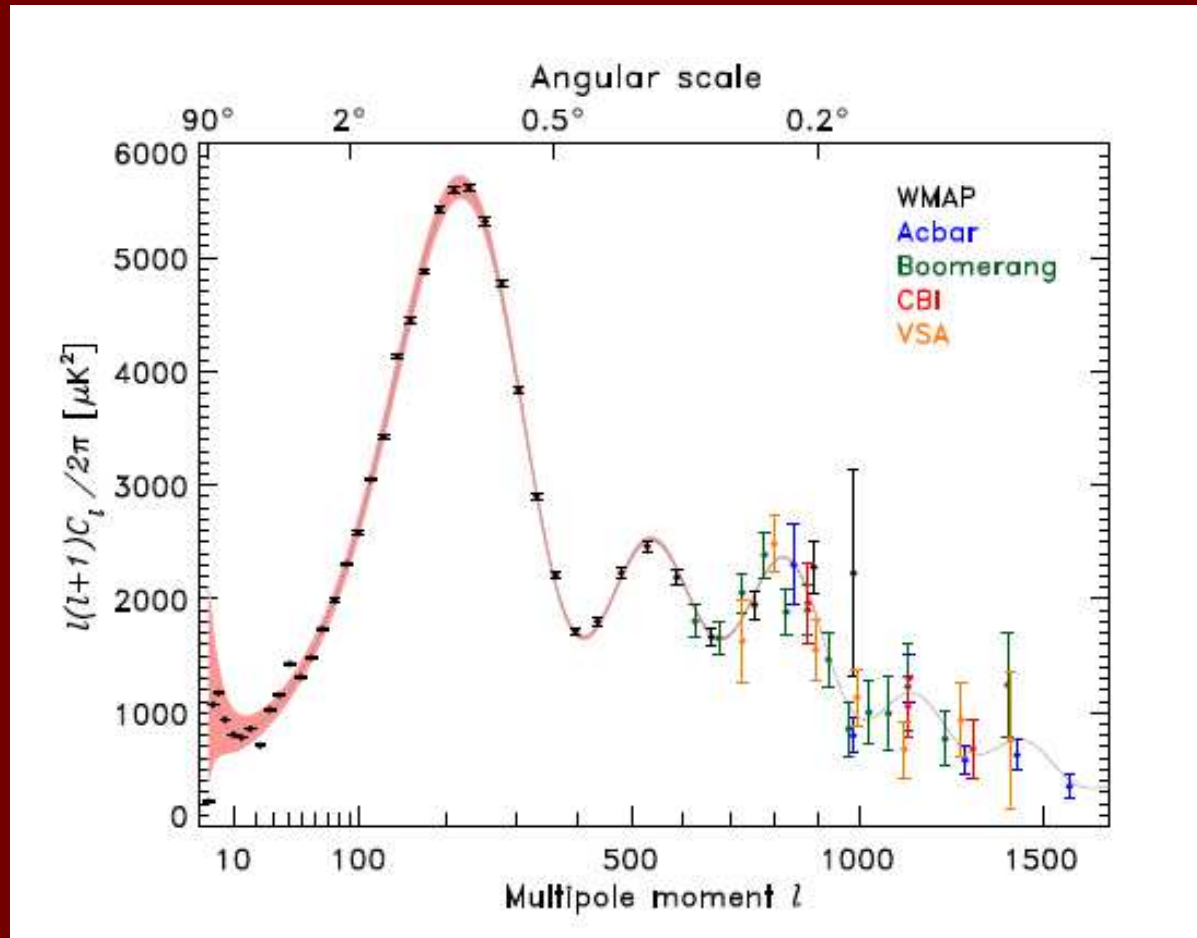
Temperature fluctuations
in the sky can be
expanded in spherical
harmonics

$$\frac{\Delta T}{T} = \sum_{\ell,m} a_{\ell}^m Y_{\ell}^m(\theta, \phi),$$

Angular power-spectrum

$$C_{\ell} = \langle |a_{\ell}^m|^2 \rangle.$$

of WMAP temperature
anisotropies



Hinshaw et al. 2006

Dark Matter & Dark Energy

Dark matter & dark energy

High-z type Ia SN data imply $q_0 < 0$, i.e. an accelerating Universe model and prefer a flat model $\Omega_0 = 1$

The first clear indication for $\Omega_0 = 1$ came from the CMB anisotropy data from the BOOMERanG and MAXIMA experiments

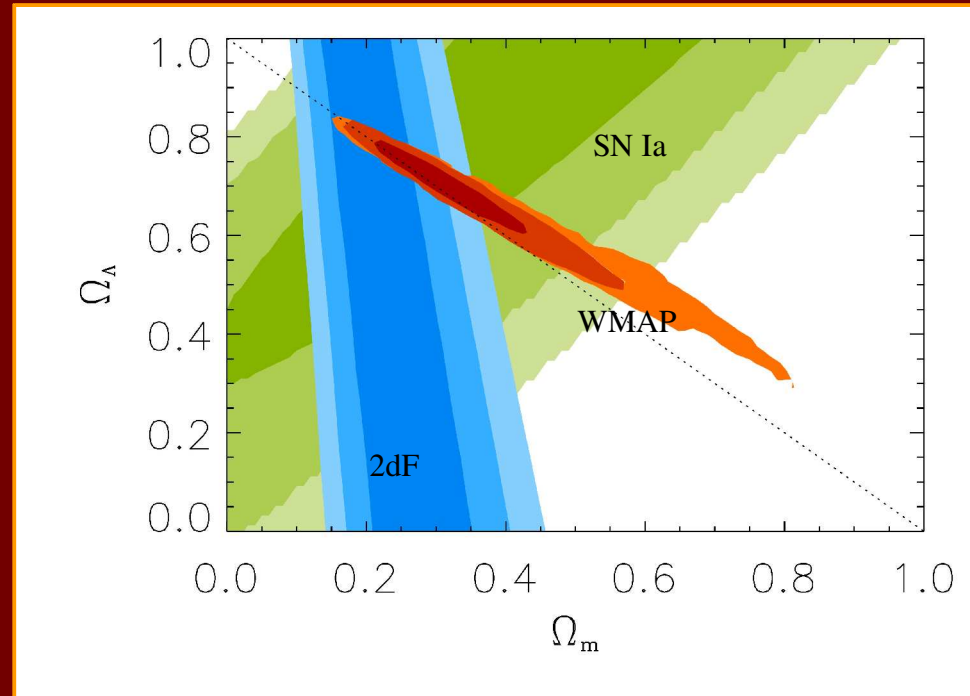
On the other hand LSS data all converge to yield a matter density parameter $\Omega_{0m} \sim 0.3$ out of which only a minor fraction can be made of baryonic matter on the basis of Big-Bang nucleosynthesis

The cosmic budget (I)

Independent datasets give a consistent determination of the amount of Dark Energy and Dark Matter in the Universe. The relative weights being measured by their density parameter

$$\Omega_i = \rho_i / \rho_c$$

where $\rho_c \approx 10^{-29} \text{ g/cm}^3$ is the *critical density* i.e. the energy density able to close the Universe



SN data: Perlmutter et al. 1998

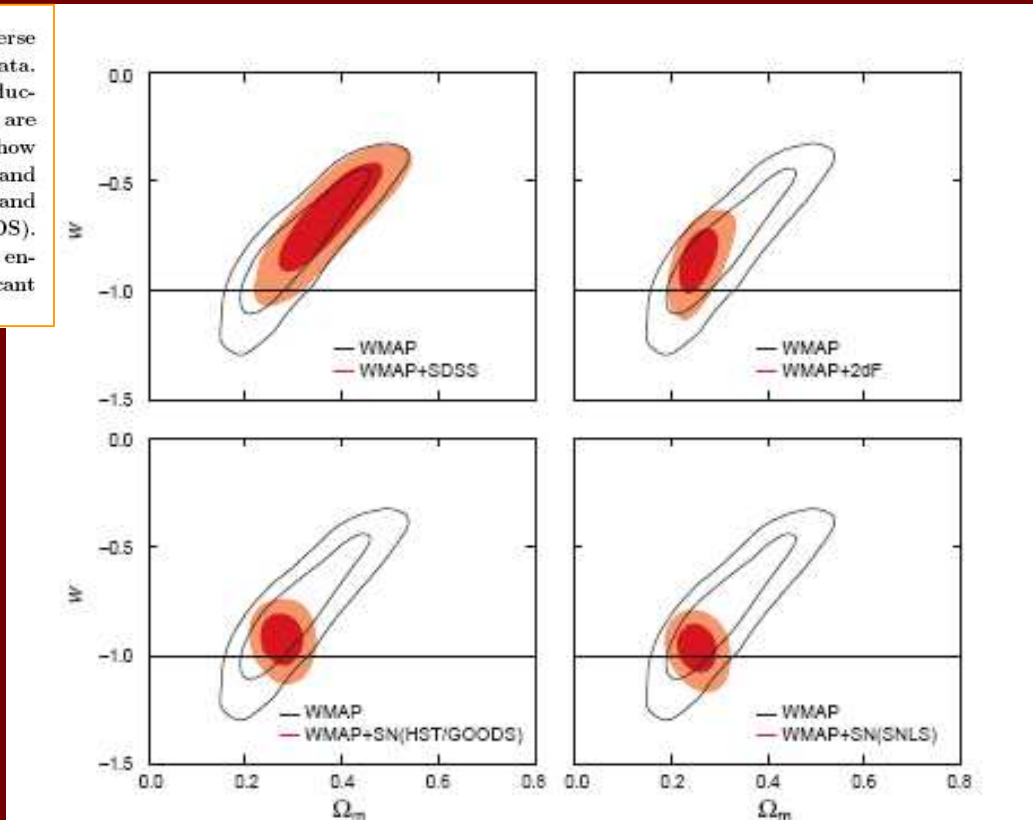
CMB data: Spergel et al. 2003

LSS data: Verde, Heavens, Percival, Matarrese & 2dF team 2002

DE properties (WMAP 3yr)

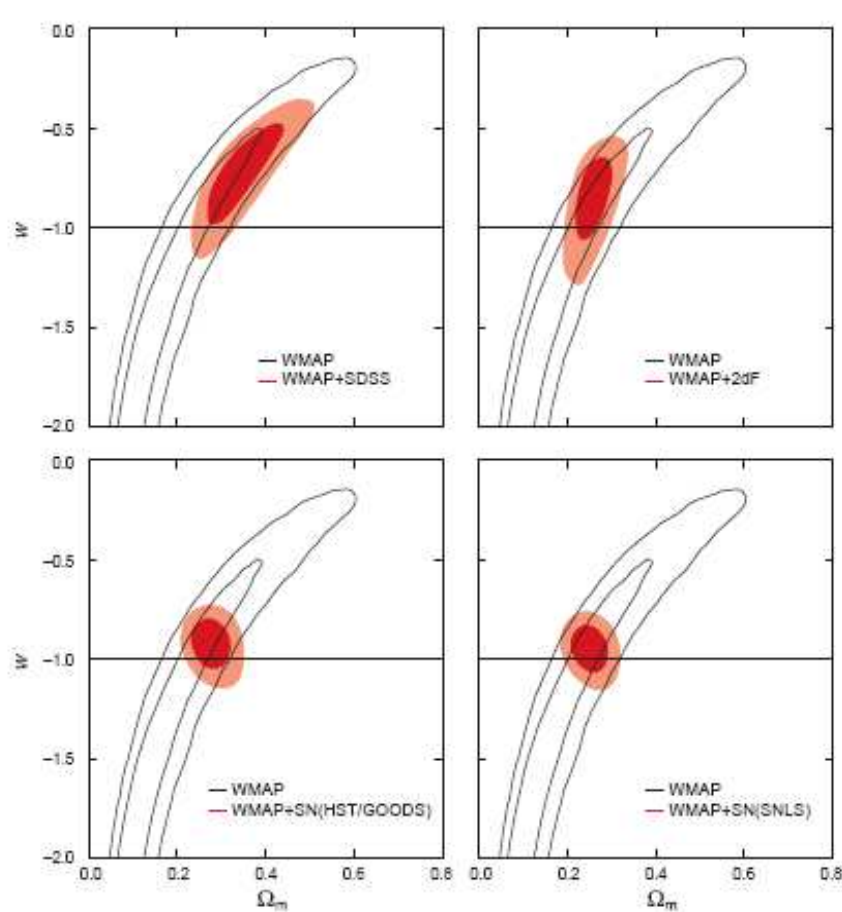
Fig. 15.— Constraints on w , the equation of state of dark energy, in a flat universe model based on the combination of WMAP data and other astronomical data. We assume that w is independent of time, and ignore density or pressure fluctuations in dark energy. In all of the figures, WMAP data only constraints are shown in blue and WMAP + astronomical data set in red. The contours show the joint 2-d marginalized contours (68% and 95% confidence levels) for Ω_m and w . (Upper left) WMAP only and WMAP + SDSS. (Upper right) WMAP only and WMAP + 2dFGRS. (Lower left) WMAP only and WMAP+SN(HST/GOODS). (Lower right) WMAP only and WMAP+SN(SNLS). In the absence of dark energy fluctuations, the excessive amount of ISW effect at $\ell < 10$ places significant constraints on the models with $w < -1$.

(Spergel et al. 2006)



DE properties (WMAP 3yr)

Fig. 16.— Constraints on w , the equation of state of dark energy, in a flat universe, Model M6 in Table 3, based on the combination of WMAP data and other astronomical data. We assume that w is independent of time, but include density and pressure fluctuations in dark energy with the speed of sound in the comoving frame equal to the speed of light, $c_s^2 = 1$. In all of the figures, WMAP data only constraints are shown in black solid lines and WMAP + astronomical data set in red. The contours show the joint 2-d marginalized contours (68% and 95% confidence levels) for Ω_m and w . (Upper left) WMAP only and WMAP + SDSS. (Upper right) WMAP only and WMAP + 2dFGRS. (Lower left) WMAP only and WMAP+SNgold. (Lower right) WMAP only and WMAP+SNLS. In the presence of dark energy fluctuations, the ISW effect at $\ell < 10$ is nearly canceled by dark energy fluctuations and thus the WMAP data alone do not place significant constraints on w .

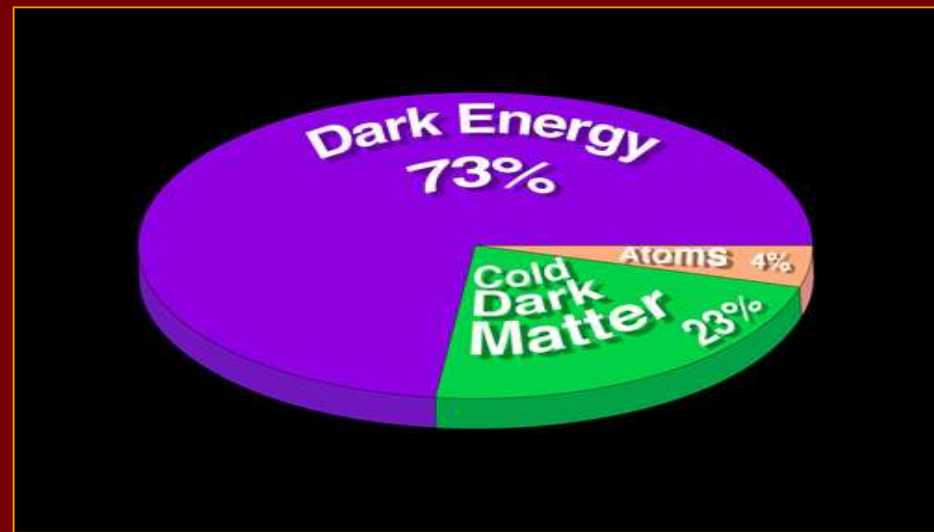


with a flat Universe prior (Spergel et al. 2006)

Cosmological Parameters (WMAP 3yr)

$\Omega_m h^2$	0.127 ± 0.010		<i>Matter density</i>
$\Omega_b h^2$	0.0223 ± 0.0008		<i>Baryon density</i>
$H_0/(100 \text{ km s}^{-1} \text{ Mpc}^{-1})$	0.73 ± 0.03		<i>Hubble constant</i>
τ	0.09 ± 0.03		<i>Optical depth</i>
σ_8	0.74 ± 0.05		<i>Amplitude of fluctuations</i>
n_s	0.951 ± 0.022		<i>Spectral index</i>
r	< 0.55	< 0.28 (+ SDSS data)	<i>Tensor to scalar ratio</i>
$\Sigma m_\nu / \text{eV}$	< 0.68		<i>Sum of neutrino masses</i>
w	-1.06 ± 0.01		<i>Dark Energy equation of state</i>
Ω_k	-0.015 ± 0.018		<i>Curvature</i>
Ω_Λ	0.072 ± 0.04	+ HST data	<i>Cosmological Constant</i>

The cosmic budget (II)



Only about 4% of the cosmic energy budget is in the form of ordinary “baryonic” matter, out of which only a small fraction shines in the galaxies (quite likely most of the baryon reside in filaments forming the Warm-Hot Intergalactic Medium (WHIM), a sort of cosmic web connecting the galaxies and clusters of galaxies).

About 23% of the cosmic budget is made of Cold Dark Matter, a collisionless component whose presence we only perceive gravitationally. The most likely candidates are particles like neutralinos (LSP), axions, WIMPZILLAs, etc....

About 73% of the energy content of our Universe is in the form of some exotic component, called Dark Energy, also called “Quintessence”, which causes a large-scale cosmic repulsion among celestial objects, thereby mimicking a sort of anti-gravity effect.

Non-baryonic dark matter

Thermal relics: particles which have been in thermal contact before their decoupling: LSP (e.g. neutralinos) belonging to the WIMP class

3. Non-thermal relics: particles which have never been in thermal equilibrium: axions, WIMPZILLAs, topological solitons, B-balls, Q-balls, self-interacting DM, DM from extra-dimensions
5. Thermal or non-thermal? Thermal DM candidates have mass bounded from above: $m < 100$ TeV. Non-thermal relics may be heavier (e.g. superheavy DM, named WIMZILLAs, gravitationally produced at the end of Inflation; Chung, Kolb & Riotto 1998; 1999)

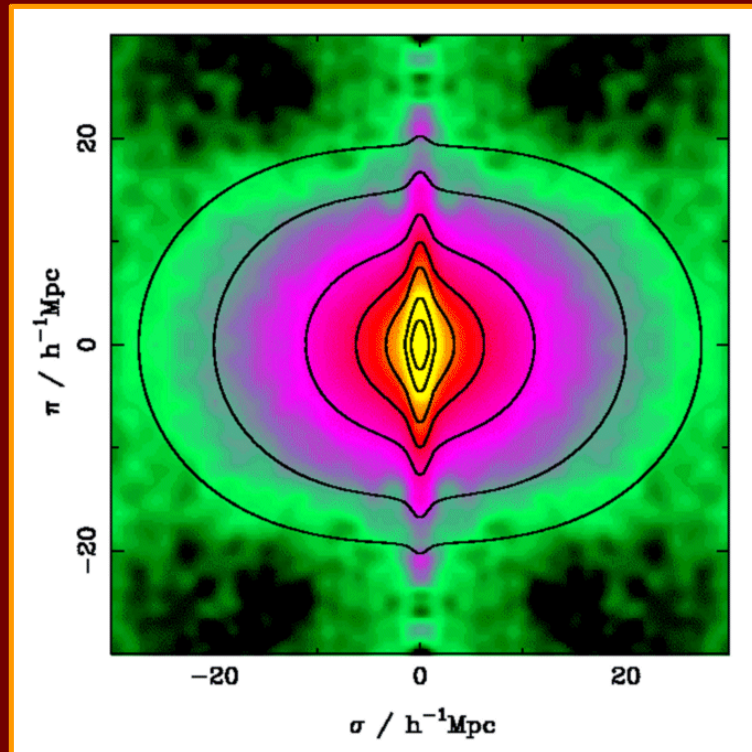
From β to Ω_m via b

The study of the galaxy redshift-space power-spectrum provides $\Omega_m^{0.6}/b$ where b is the bias factor defined by

$$\delta_{\text{galaxies}} = b \delta_{\text{mass}} + b_2 \delta_{\text{mass}}^2$$

There is a degeneracy intrinsic to linear theory (i.e. of power-spectrum studies)

→ need b to get Ω_m



Peacock et al. (2dF team) 2001

$$\Omega_m^{0.6} / b = 0.43 \pm 0.07$$

Bias and Ω_0 from the 2dFGRS

Analysing the bispectrum of 2dF galaxies

Verde, Heavens, Percival, Matarrese &
2dF
team (2002) find

$$b \approx 1.04 \pm 0.11$$

$$b_2 \approx 0.05 \pm 0.08$$

(in very good agreement with independent analysis by Lahav et al. 2002)

No scale dependence of bias is found

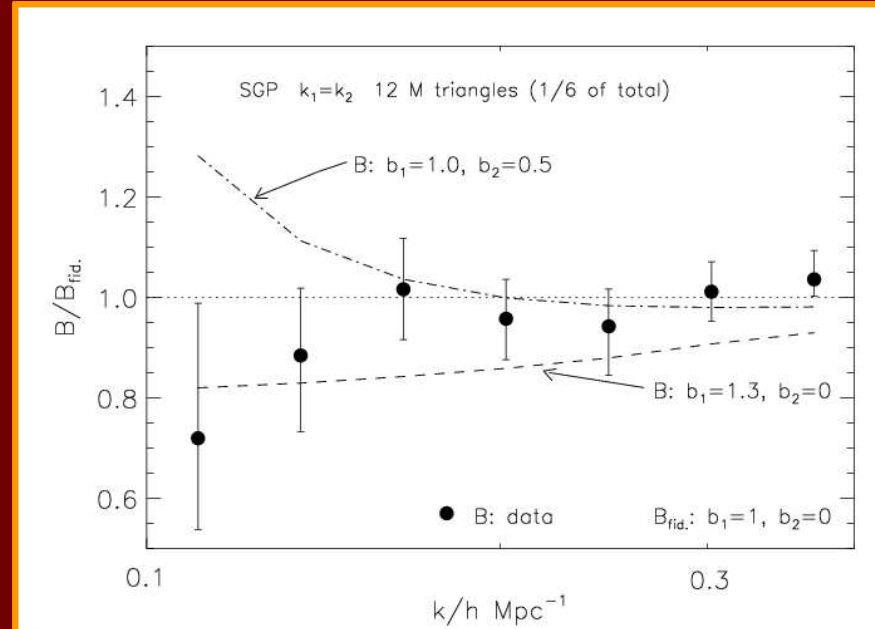
Using the 2dF determination (Peacock et al. 2001)

$$\frac{m}{b} \approx 0.6$$



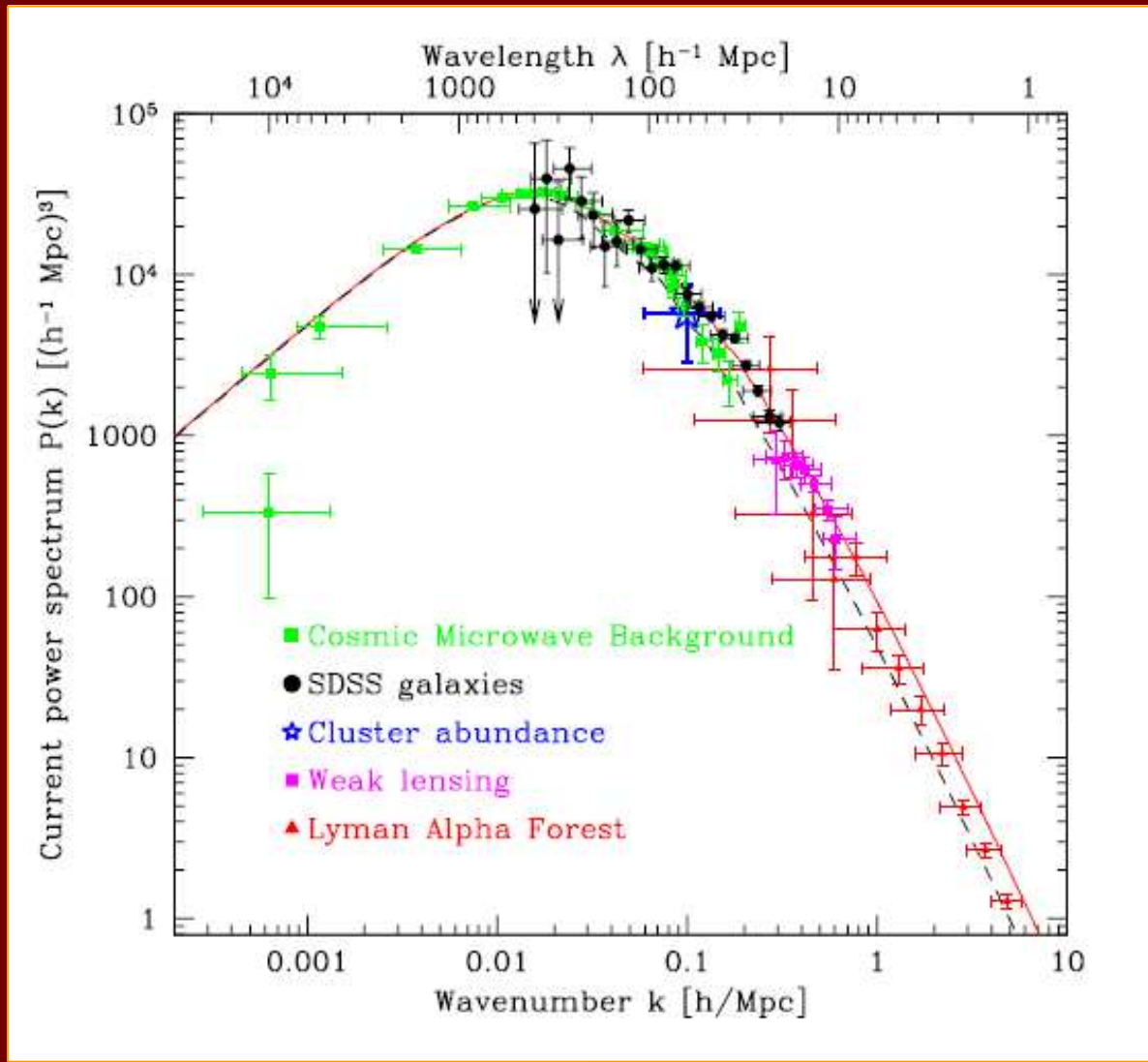
$$\begin{aligned} m &\approx 0.27 \pm 0.06 \\ 0.13 &\approx m_0 \approx 0.27 \end{aligned}$$

$\Omega_m \approx 0.27 \pm 0.06$
 $z \sim 0.17$
 $z=0$



Success of the “concordance” model

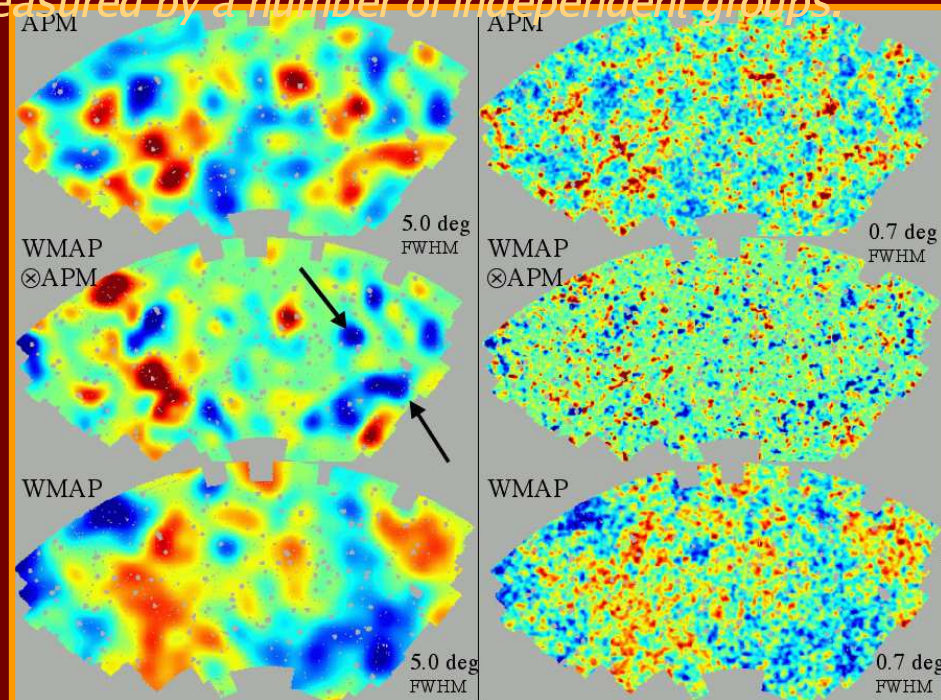
The predicted power-spectrum of density fluctuations of the Lambda Cold Dark Matter (Λ CDM) or “concordance” model fits a variety of independent datasets spanning more than four decades in scale



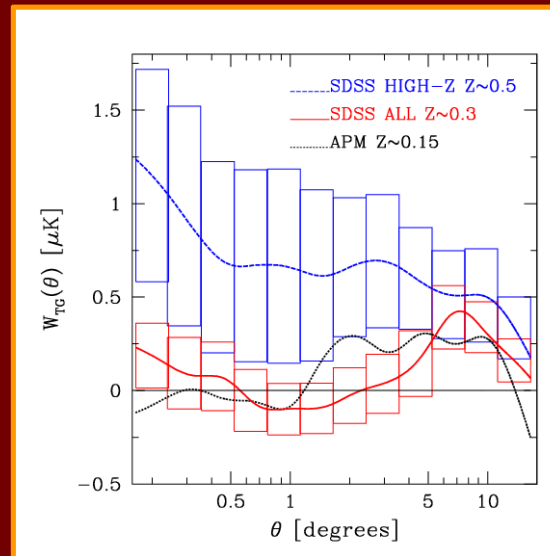
CMB-LSS cross-correlations: evidence for dark energy

ISW (Rees-Sciama) effect: a time variation of the gravitational potential at recent times, as it may arise from the presence of dark energy, induces excess temperature anisotropy at low l . The same gravitational potential is responsible for structure formation, then a cross-correlation is predicted between CMB anisotropies and LSS data. This effect has been recently

measured by a number of independent groups



Fosalba et al. 2003



The Cosmological Constant Problem

geometry

matter

$$G_{\square} + g_{\square} = 8\pi G T_{\square}$$

$$\frac{\dot{G}_{\square}}{G_{\square}} \approx \frac{i\dot{\zeta}^{1/2}c}{8} \approx 0.7 i\dot{\zeta}^{1/2} \approx 10^{148} \text{ GeV}^4 \approx 10^{124} m_{\text{Planck}}^4$$
$$m_{\text{Planck}} \approx G^{1/2} \approx 10^{19} \text{ GeV}$$

Λ vs. Quintessence I

□ □ 0 and constrained by observations has two main problems:

□ *fine-tuning: why is Λ so small?*

□ *cosmic coincidence: why different forms of energy (DE, DM, baryons) have comparable abundance today?*

Λ vs. Quintessence !!

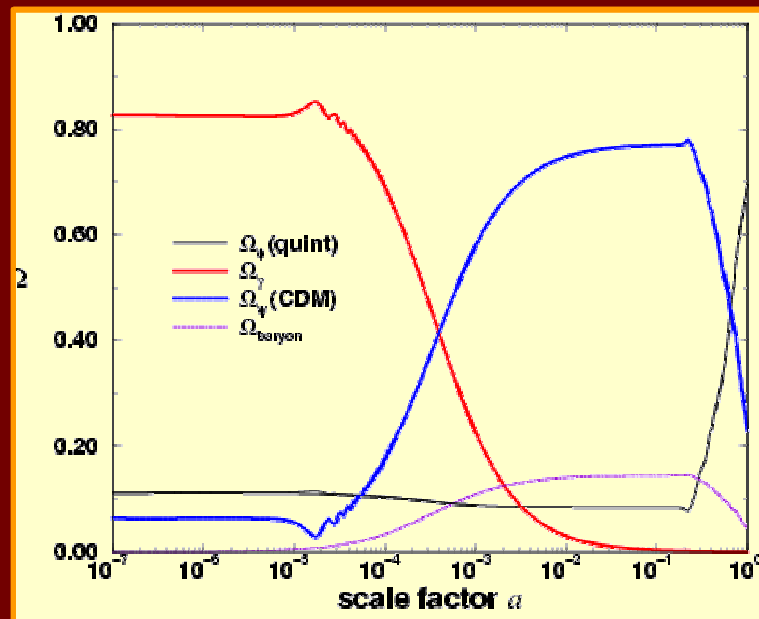
The Quintessence is a hypothetical

*fifth ingredient of the Universe
made of a slowly rolling and nearly
homogeneous scalar field Q with
typical potential $V(Q) \sim Q^{-\alpha}$ (Ratra
& Peebles 1988), leading to a
(mean) equation of state $p=w\rho$,
with ($w < -1/3$) and (unnaturally?)
tiny mass*

$$m_Q \sim H_0 \sim 10^{-33} \text{ eV} \quad !!$$

Wednesday, October 11, 200

FPS-06 Frascati



Sahni 2002

21

Dark energy models

Quintessence: tracking scalar fields (Ratra & Peebles 1988; Wetterich 1988; Coble et al. 1997; Ferreira & Joyce 1998; Liddle & Scherrer 1999; Steinhardt et al. 1999; Brax & Martin 2000; Doran et al. 2001; ...)

^{3.} Extended Quintessence: non-minimal coupling to Gravity (Chiba 1999; Uzan 1999; Perrotta et al. 2000; Baccigalupi et al. 2000; Bartolo & Pietroni 2000; Esposito-Farese & Polarski 2001; ...)

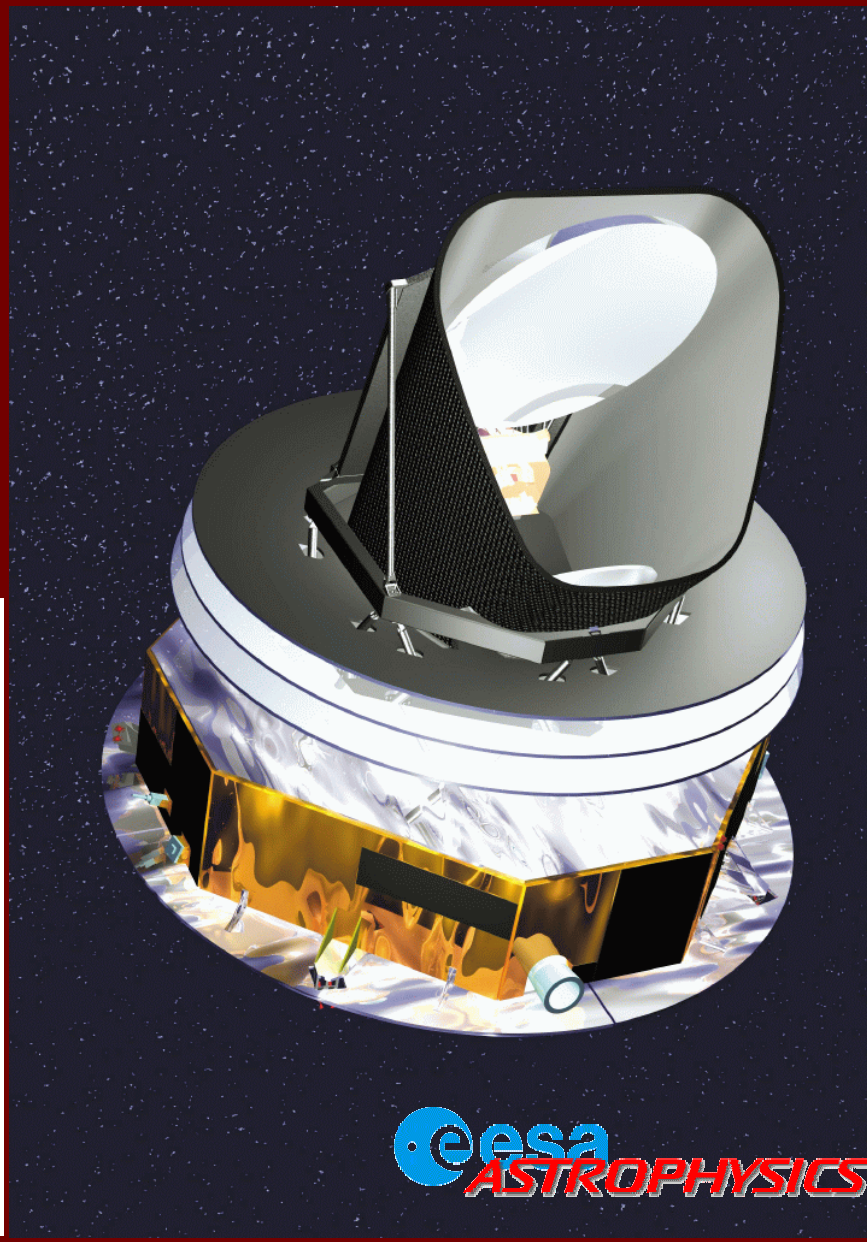
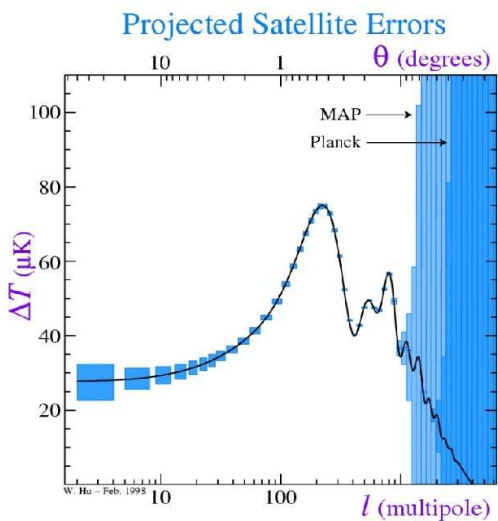
^{5.} Coupled Quintessence: coupling with dark matter (Carroll 1998; Amendola 2000; Comelli et al. 2003; Matarrese et al. 2003; Fahri & Peebles 2003 ...)

^{7.} k-essence: modified kinetic scalar field energy (Amendariz-Picon et al. 2001; Mukhanov 2001; Malquarti et al. 2003)

^{9.} Chaplygin gas: dark matter and energy described by a single gas having equation of state $p=-A/\rho$ (Gorini et al. 2001; Bilic et al. 2001; ...)

PLANCK

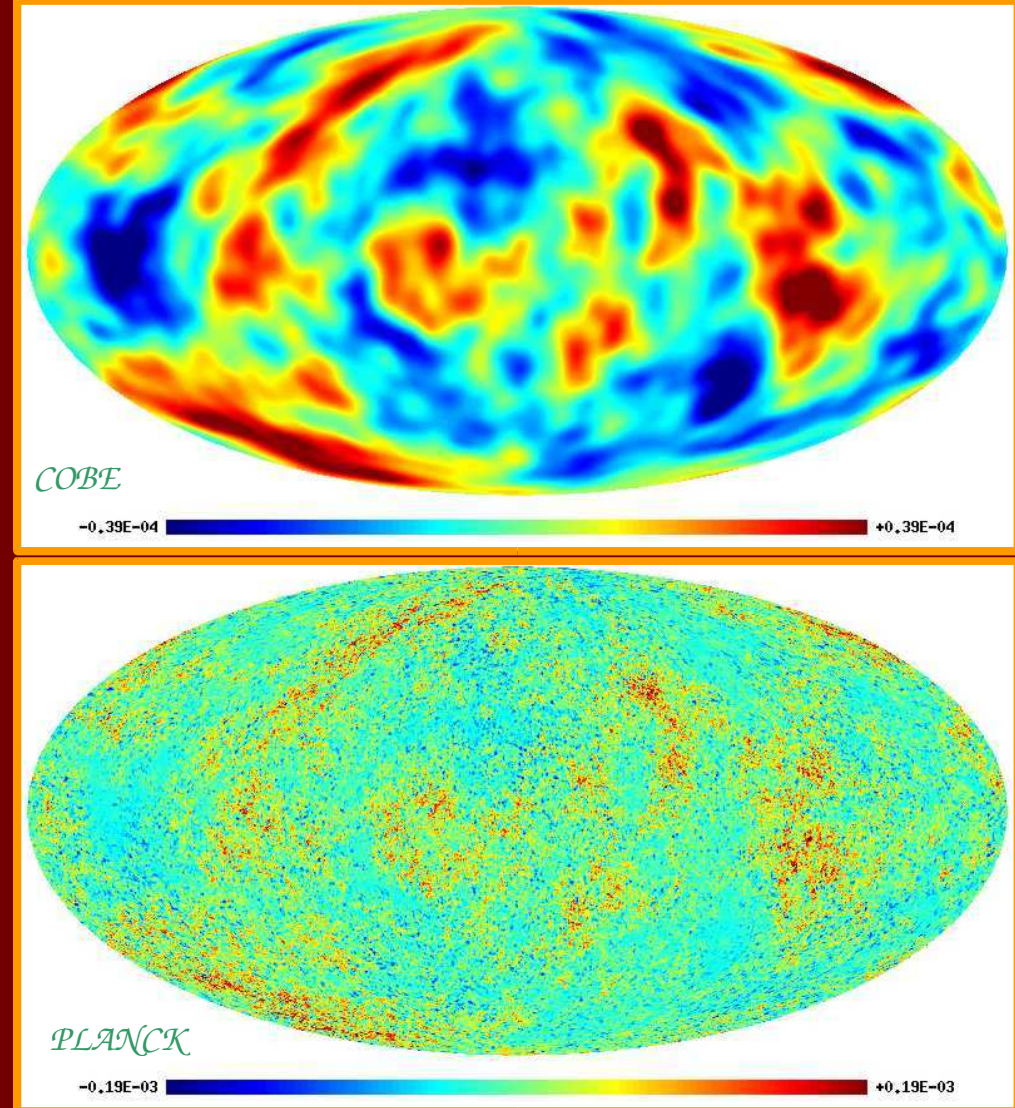
The Planck Surveyor, which will be launched in 2007 by ESA, is a satellite to measure the temperature anisotropy and polarization of the CMB with unprecedented resolution



PLANCK



The basic scientific goal of the PLANCK mission is to measure the CMB anisotropies at all angular scales larger than 10 arcminutes, with an accuracy set by astrophysical limits.



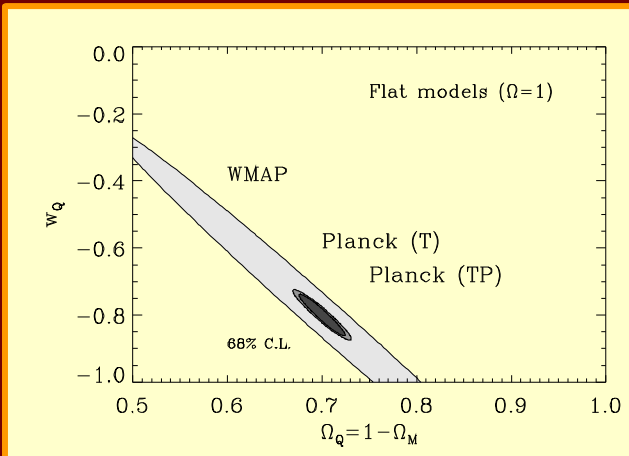
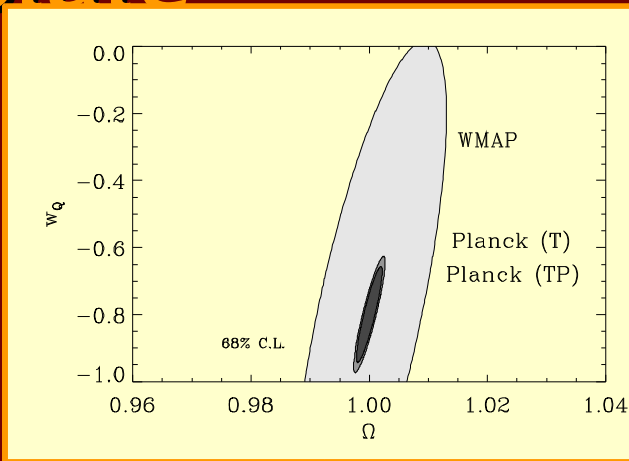
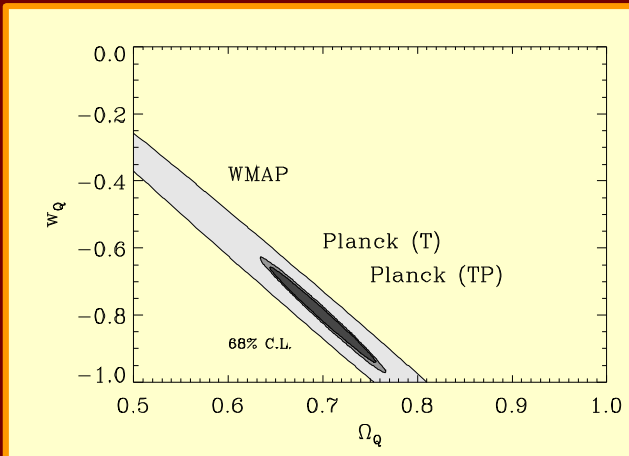
Simulated maps of CMB anisotropies expected in a Λ CDM model.
Upper panel: a simulated COBE map with a resolution of $\vartheta_{\text{FWHM}} = 7^\circ$.
Lower panel: the same realization of the sky at the much higher angular resolution and signal-to-noise of PLANCK (Liguori, Matarrese & Moscardini 2003).

Determining the dark energy equation of state

The DE density parameter Ω_{DE} and equation of state w_{DE} will be determined with high precision (better than 10%) by the combination of CMB data (Planck) and type Ia SN redshift measurements (SNAP)

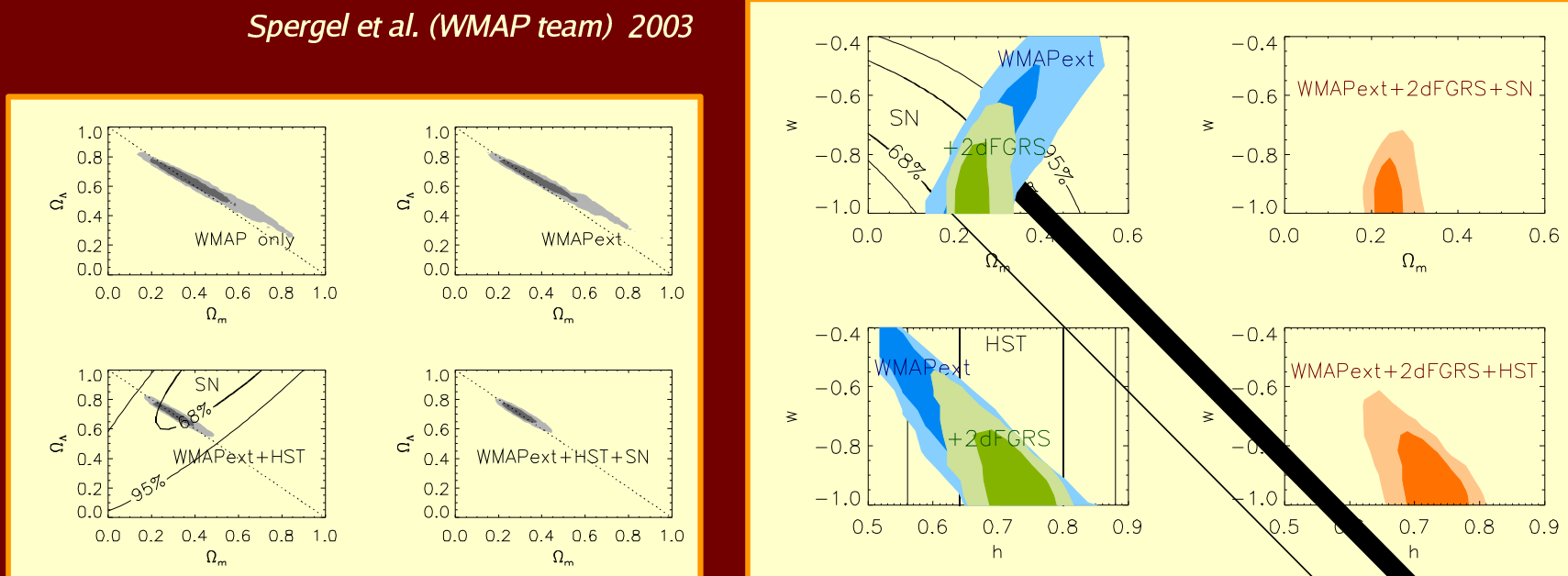
CMB: Balbi, Baccigalupi, Matarrese, Perrotta & Vittorio 2003

SN: Caresia, Matarrese & Moscardini 2003



WMAP constraints on Ω_{DE} and w_{DE}

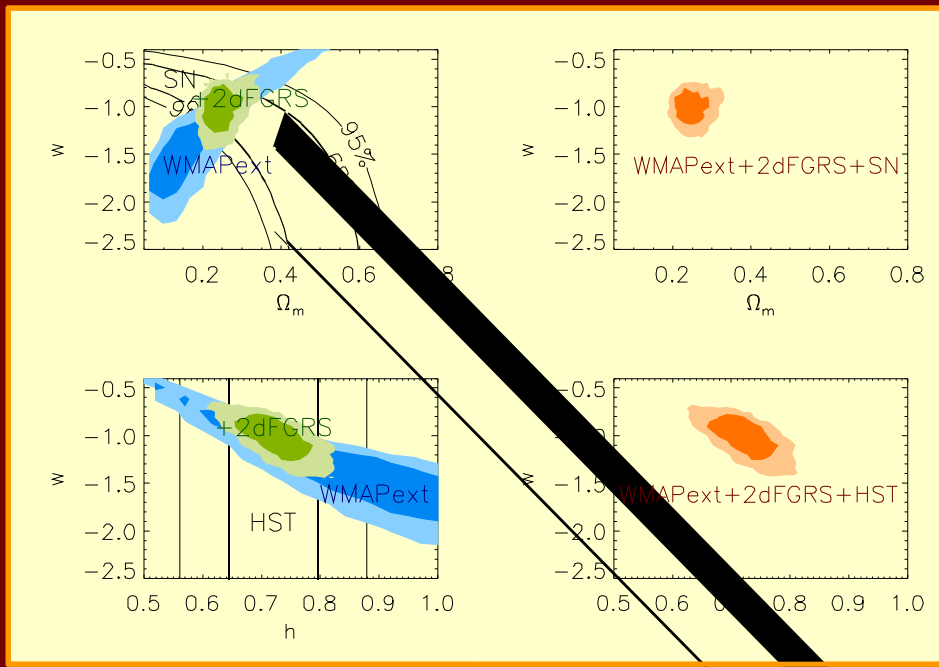
The WMAP extended dataset allows to put quite strong constraints on the dark energy density parameter $\Omega_{DE} = \rho_{DE}/\rho_c$ while the precise value of its equation of state $w_{DE} = p_{DE}/\rho_{DE}$ is still poorly known. We only know that w is close to -1 (the cosmological constant case) and we know almost nothing on its time evolution



Is the “weak energy condition” violated? (a “phantom” field)

□ The data seem to favour $w < -1$, or $p < -\rho$, i.e. a violation of the weak energy condition!

3. At present there are no convincing physical models able to account for this property

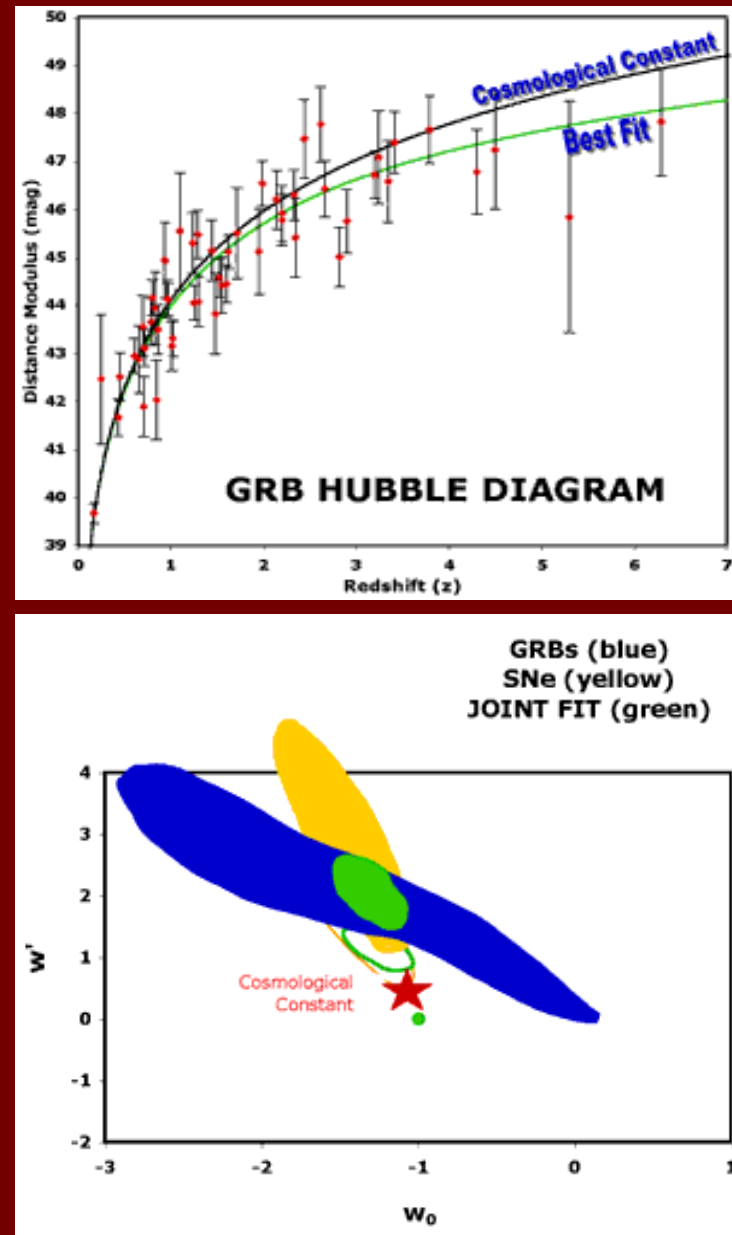


Spergel et al. (WMAP team) 2003

DE equation of state from high-z observations

The Hubble Diagram places constraints on the allowed cosmology, here represented by the parameters w_0 and w' which express the current 'equation of state' of the Universe and how it varies with time. Einstein's Cosmological Constant is the case where $w_0=-1$ and $w'=0$ (indicated with the red star). The yellow region shows the allowed parameters based on supernovae alone, the blue region shows the constraints from Gamma-Ray Bursts alone, and the green region is the joint allowed region. These regions all represent the 67% CL. The red star falls outside the blue and green regions, the implication of this being that the Cosmological Constant appears to be rejected.

Schaefer et al. 2006

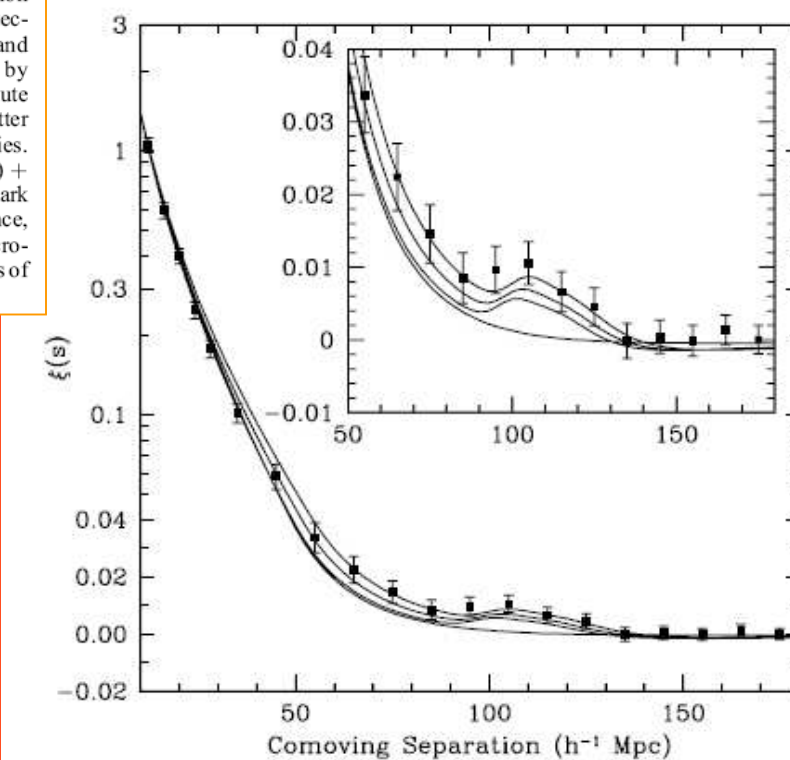


Baryonic wiggles in LSS

Eisenstein et al. have detected a clear signal of acoustic oscillations in the SDSS galaxy two-point function

We present the large-scale correlation function measured from a spectroscopic sample of 46,748 luminous red galaxies from the Sloan Digital Sky Survey. The survey region covers $0.72 h^{-3} \text{ Gpc}^3$ over 3816 deg^2 and $0.16 < z < 0.47$, making it the best sample yet for the study of large-scale structure. We find a well-detected peak in the correlation function at $100 h^{-1} \text{ Mpc}$ separation that is an excellent match to the predicted shape and location of the imprint of the recombination-epoch acoustic oscillations on the low-redshift clustering of matter. This detection demonstrates the linear growth of structure by gravitational instability between $z \approx 1000$ and the present and confirms a firm prediction of the standard cosmological theory. The acoustic peak provides a standard ruler by which we can measure the ratio of the distances to $z = 0.35$ and $z = 1089$ to 4% fractional accuracy and the absolute distance to $z = 0.35$ to 5% accuracy. From the overall shape of the correlation function, we measure the matter density $\Omega_m h^2$ to 8% and find agreement with the value from cosmic microwave background (CMB) anisotropies. Independent of the constraints provided by the CMB acoustic scale, we find $\Omega_m = 0.273 \pm 0.025 + 0.123(1 + w_0) + 0.137\Omega_K$. Including the CMB acoustic scale, we find that the spatial curvature is $\Omega_K = -0.010 \pm 0.009$ if the dark energy is a cosmological constant. More generally, our results provide a measurement of cosmological distance, and hence an argument for dark energy, based on a geometric method with the same simple physics as the microwave background anisotropies. The standard cosmological model convincingly passes these new and robust tests of its fundamental properties.

FIG. 2.—Large-scale redshift-space correlation function of the SDSS LRG sample. The error bars are from the diagonal elements of the mock-catalog covariance matrix; however, the points are correlated. Note that the vertical axis mixes logarithmic and linear scalings. The inset shows an expanded view with a linear vertical axis. The models are $\Omega_m h^2 = 0.12$ (top line), 0.13 (second line), and 0.14 (third line), all with $\Omega_b h^2 = 0.024$ and $n = 0.98$ and with a mild non-linear prescription folded in. The bottom line shows a pure CDM model ($\Omega_m h^2 = 0.105$), which lacks the acoustic peak. It is interesting to note that although the data appear higher than the models, the covariance between the points is soft as regards overall shifts in $\xi(s)$. Subtracting 0.002 from $\xi(s)$ at all scales makes the plot look cosmetically perfect but changes the best-fit χ^2 by only 1.3. The bump at $100 h^{-1} \text{ Mpc}$ scale, on the other hand, is statistically significant. [See the electronic edition of the Journal for a color version of this figure.]



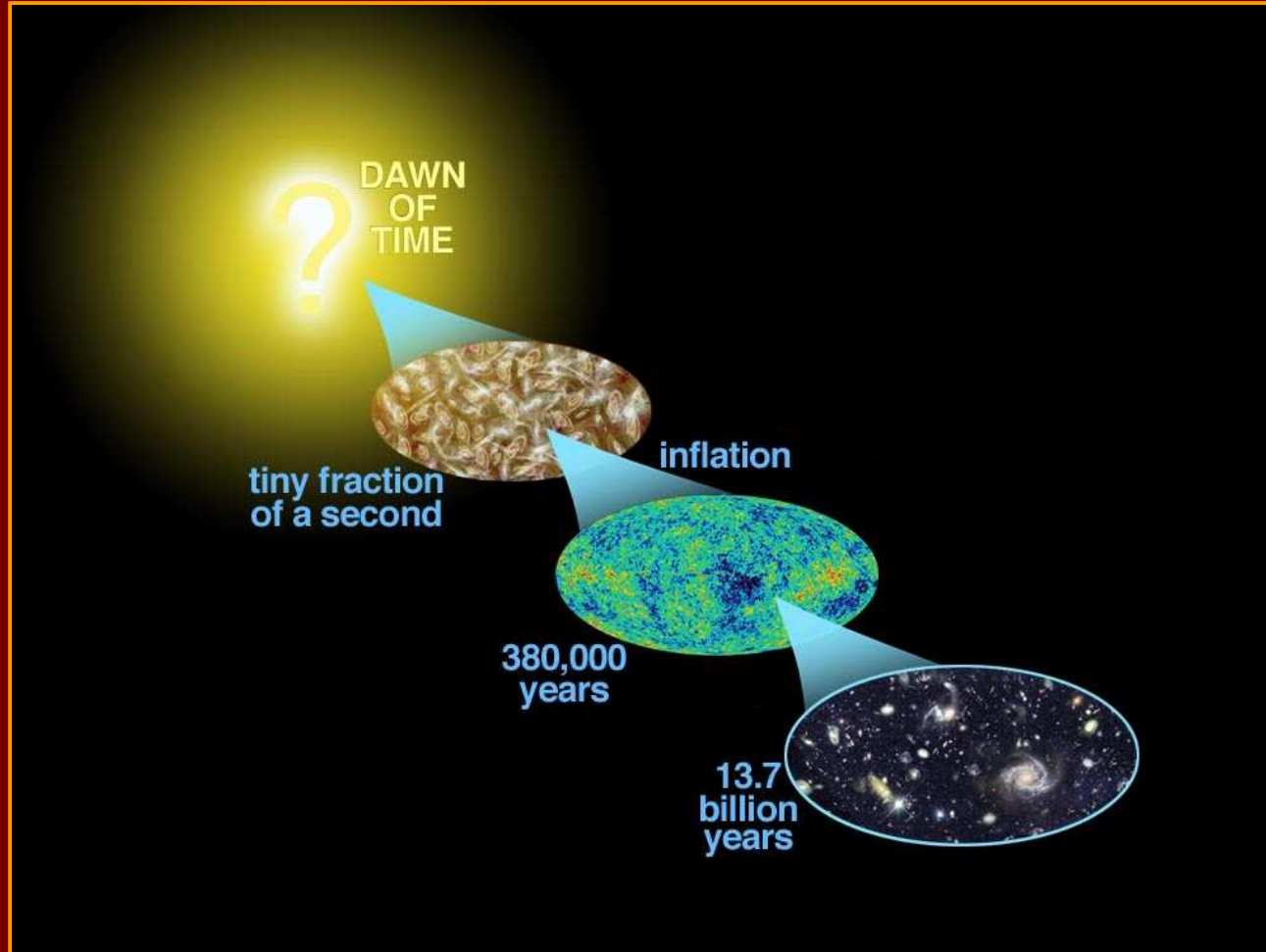
Inflation in the Early Universe

Inflation in the Universe

The seeds of structure formation in the Universe were generated in the early Universe, during an epoch of accelerated expansion, i.e.



named Inflation



The role of vacuum energy

To realize a physical system with negative isotropic

pressure (“tension”) one needs to make use of the properties of the vacuum state in QFT. A well-known example being the Casimir effect in QED.

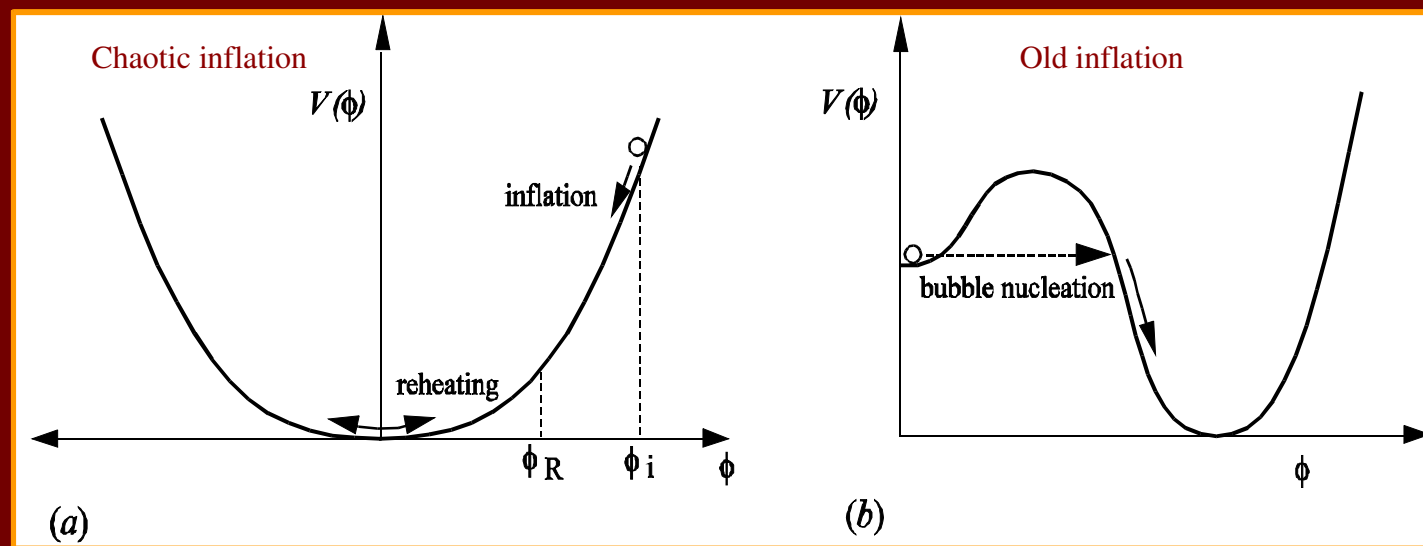
$$a \equiv 0 \quad p \equiv -\frac{1}{3}c^2$$



scalar field dynamics

New vs. Old Inflation dynamics

Different models of inflation derive from different potential and different initial conditions. Old inflation (Guth 1981) assumes thermal initial conditions (which are very difficult to achieve). Chaotic inflation (Linde 1983) is based on the application of the uncertainty principle at Planck energies.

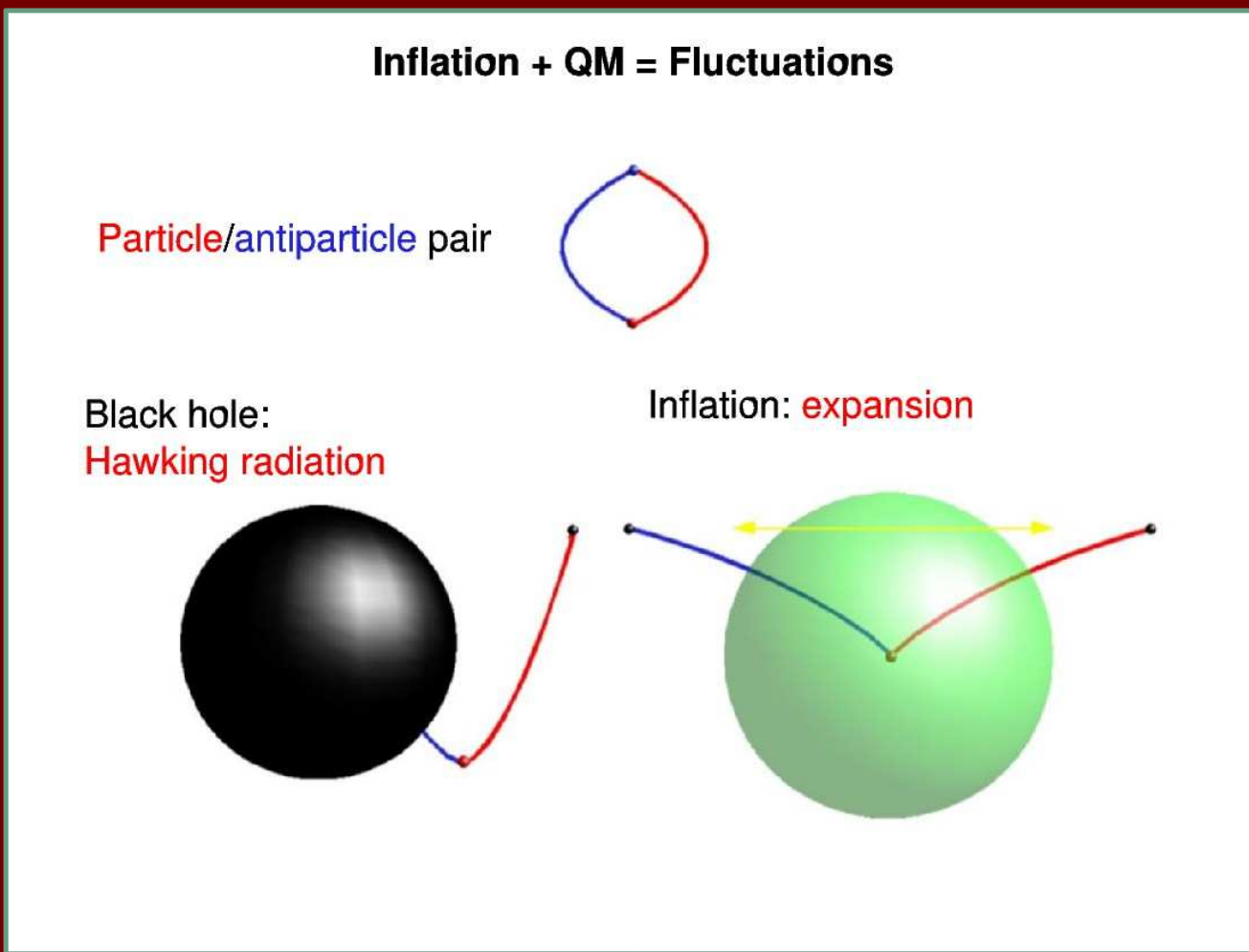


The primordial seeds

Particle creation in either
strong (Hawking 1972)
or rapidly varying
(Parker 1969)
gravitational fields

Schrodinger (1939): “an_ alarming phenomenon”.

In QED the analogous effect in a strong electric field is known as “Klein paradox”



Kinney 2003

Classify Inflationary Models

The shape of the inflaton potential $V(\phi)$ determines the observables.

slow-roll conditions

It is standard to use three parameters to characterize the shape:

“slope” of the potential $(V'/V)^2 \ll 1$

“curvature” of the potential $|V''/V| \ll 1$

“jerk” of the potential $(V'/V)(V''/V) \sim \epsilon^2$

Slow-roll parameters and observables

$$\epsilon = \frac{M_P^2}{2} \left(\frac{V'}{V} \right)^2$$

$$\Box^2 \Box M_P^2 V' V''' / V^2$$

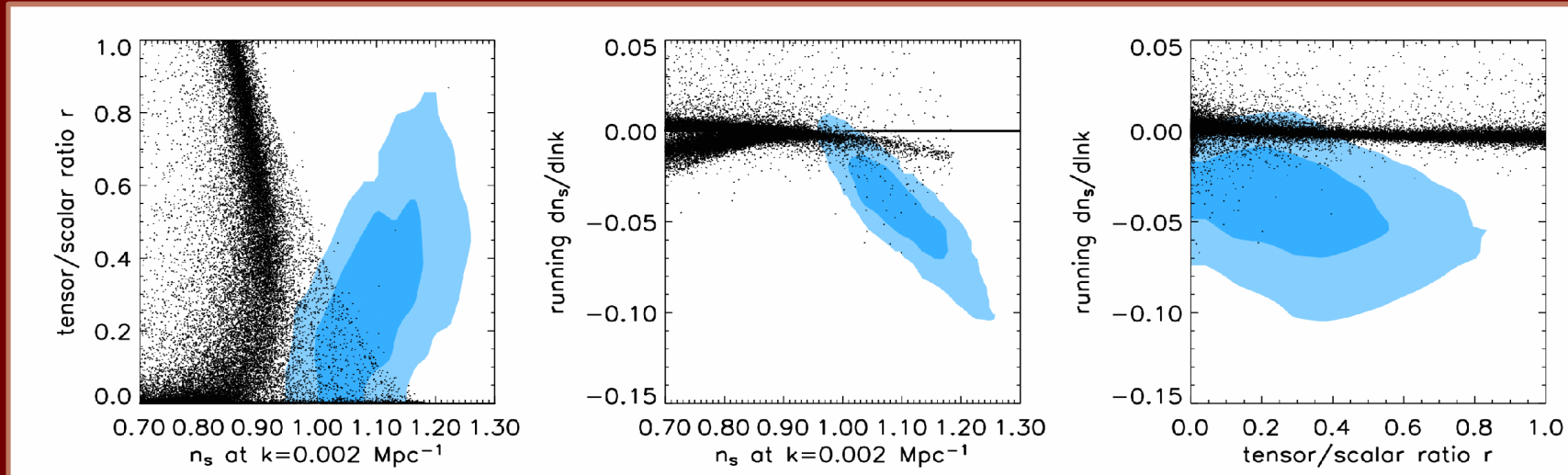
$$M_P \equiv (8\pi G_N)^{-1/2} :$$

$$\eta = M_P^2 \left(\frac{V''}{V} \right)$$

Scalar (comoving curvature)
perturbation power-spectrum

$$\left\{ \begin{array}{l} \mathcal{P}_{\mathcal{R}}(k) = \frac{1}{2M_P^2 \epsilon} \left(\frac{H_*}{2\pi} \right)^2 \left(\frac{k}{aH_*} \right)^{n_{\mathcal{R}}-1} \quad \left\{ \begin{array}{l} n_{\mathcal{R}} \Box 1 \Box 6 \Box 2 \\ dn_{\mathcal{R}} / d \ln k \Box 2 \Box 16 \Box 24 \Box^2 \end{array} \right. \\ \mathcal{P}_T(k) = \frac{k^3}{2\pi^2} \langle h_{ij}^* h^{ij} \rangle = \frac{8}{M_P^2} \left(\frac{H_*}{2\pi} \right)^2 \left(\frac{k}{aH_*} \right)^{n_T} \quad \left\{ \begin{array}{l} r = \frac{\mathcal{P}_T}{\mathcal{P}_{\mathcal{R}}} = 16\epsilon \\ n_T = -2\epsilon \end{array} \right. \end{array} \right.$$

“Generic” predictions of single field slow-roll models vs. WMAP



Peiris et al. 2003

Each point is a “viable” slow-roll model, able to sustain inflation for sufficient e-foldings to solve the horizon problem and make the Universe (nearly) flat.

Monte Carlo simulations following Kinney (2002) flow-equation technique

Testable predictions of inflation

□ Cosmological aspects

- Critical density Universe
- Almost scale-invariant, adiabatic and nearly Gaussian density fluctuations
- Stochastic background of gravitational waves with almost scale-invariant spectrum

6. Particle physics aspects

- Origin of the inflaton
- Inflation energy scale

Key Inflationary predictions

Almost scale-invariant initial density fluctuations

Stochastic gravitational-wave background

Mild deviations of density perturbations from gaussianity

Primordial gravitational waves (I)

GWs are tensor perturbations of the metric. Restricting ourselves to a flat FRW background (and disregarding scalar and vector modes)

$$ds^2 = a^2(\tau)[d\tau^2 - (\delta_{ij} + h_{ij}(x, \tau)) dx^i dx^j]$$

where h_{ij} are tensor modes which have the following properties

$$h_{ij} = h_{ji} \quad (\text{symmetric})$$

$$h_i^i = 0 \quad (\text{traceless})$$

$$h_{jli}^i = 0 \quad (\text{transverse})$$

and satisfy the equation of motion

$$h''_{ij} - 2\frac{a'}{a}h'_{ij} - 2h_{ij}'' - S_{ij}$$

Possible source term. It vanishes in linear theory and for a perfect fluid.

$$' = d/d\tau$$

Primordial gravitational waves (II)

GWs have only (96-1-3=) two independent degrees of freedom, corresponding to the two polarization states of the graviton

$$h_{ij}(x, t) = \frac{d^3 k}{(2\pi)^3} e^{ik \cdot x} h_{ij}(k)$$

$\Box'' \Box 2 \frac{a'}{a} \Box' \Box k^2 \Box \Box 0$

polarization tensor

free massless, minimally coupled scalar field

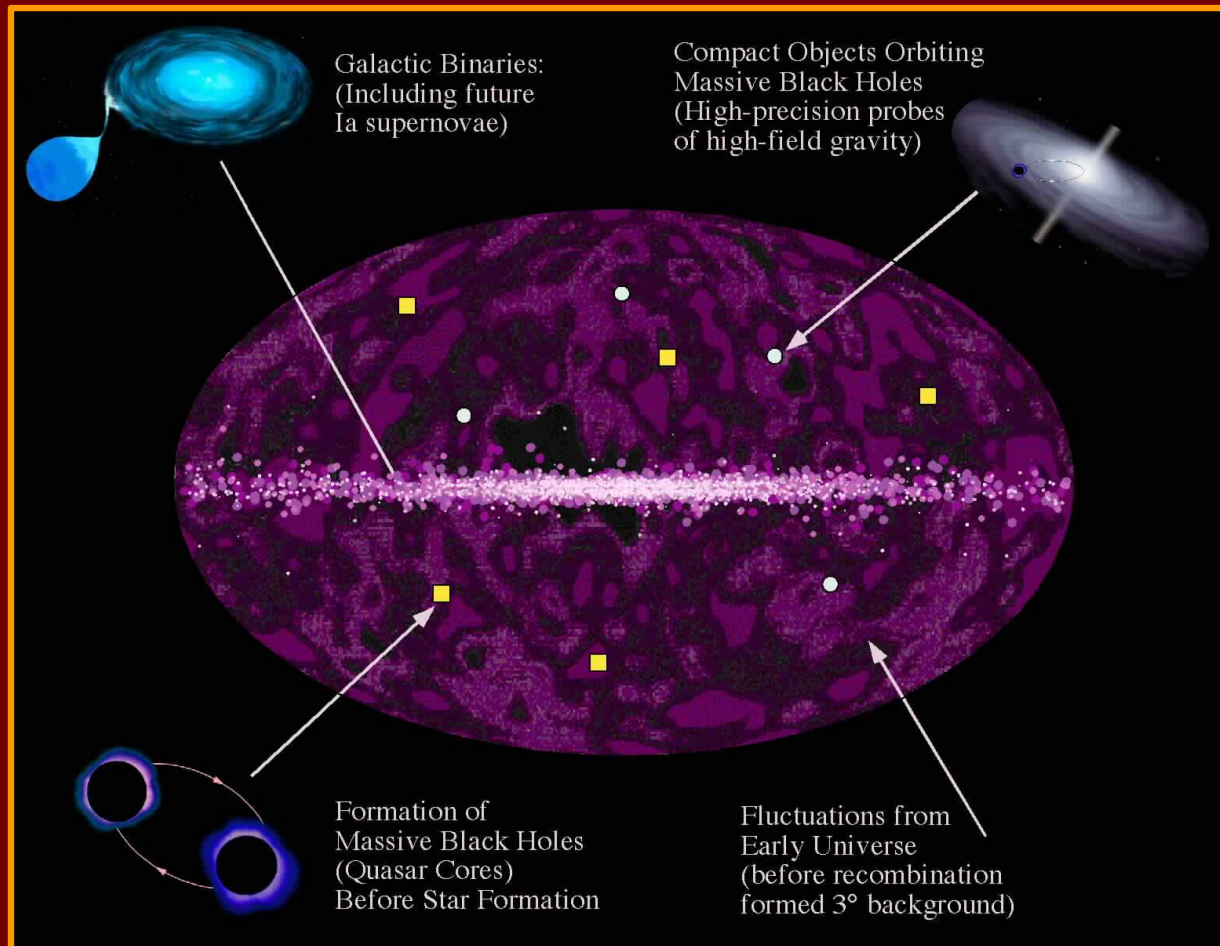
The diagram illustrates the decomposition of the metric perturbation $h_{ij}(x, t)$ into a sum over momentum k . It shows the expression $h_{ij}(x, t) = \frac{d^3 k}{(2\pi)^3} e^{ik \cdot x} h_{ij}(k)$. Below this, a condition is given: $\Box'' \Box 2 \frac{a'}{a} \Box' \Box k^2 \Box \Box 0$. To the right, two green boxes define terms: 'polarization tensor' and 'free massless, minimally coupled scalar field'. Arrows point from these labels to the $e^{ik \cdot x}$ term and the $h_{ij}(k)$ term respectively.

behaviour:

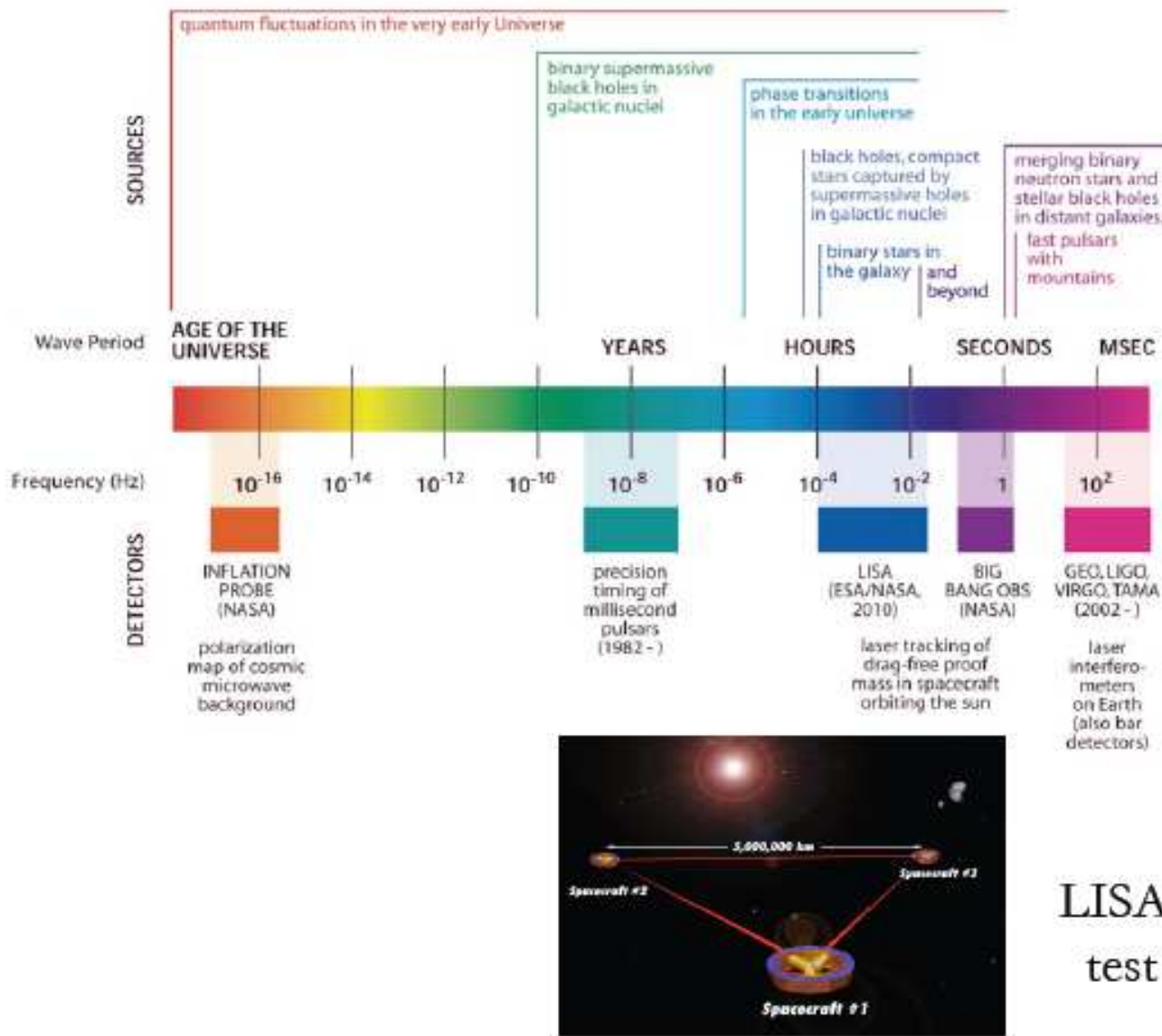
$k \ll aH$ (outside the horizon) $\phi \approx \text{const} + \text{decaying mode}$

$k \gg aH$ (inside the horizon) $\phi \approx e^{\pm ik\tau}/a$ (gravitational wave; it freely streams, experiencing redshift and dilution, like a free photon)

Sources of GWs

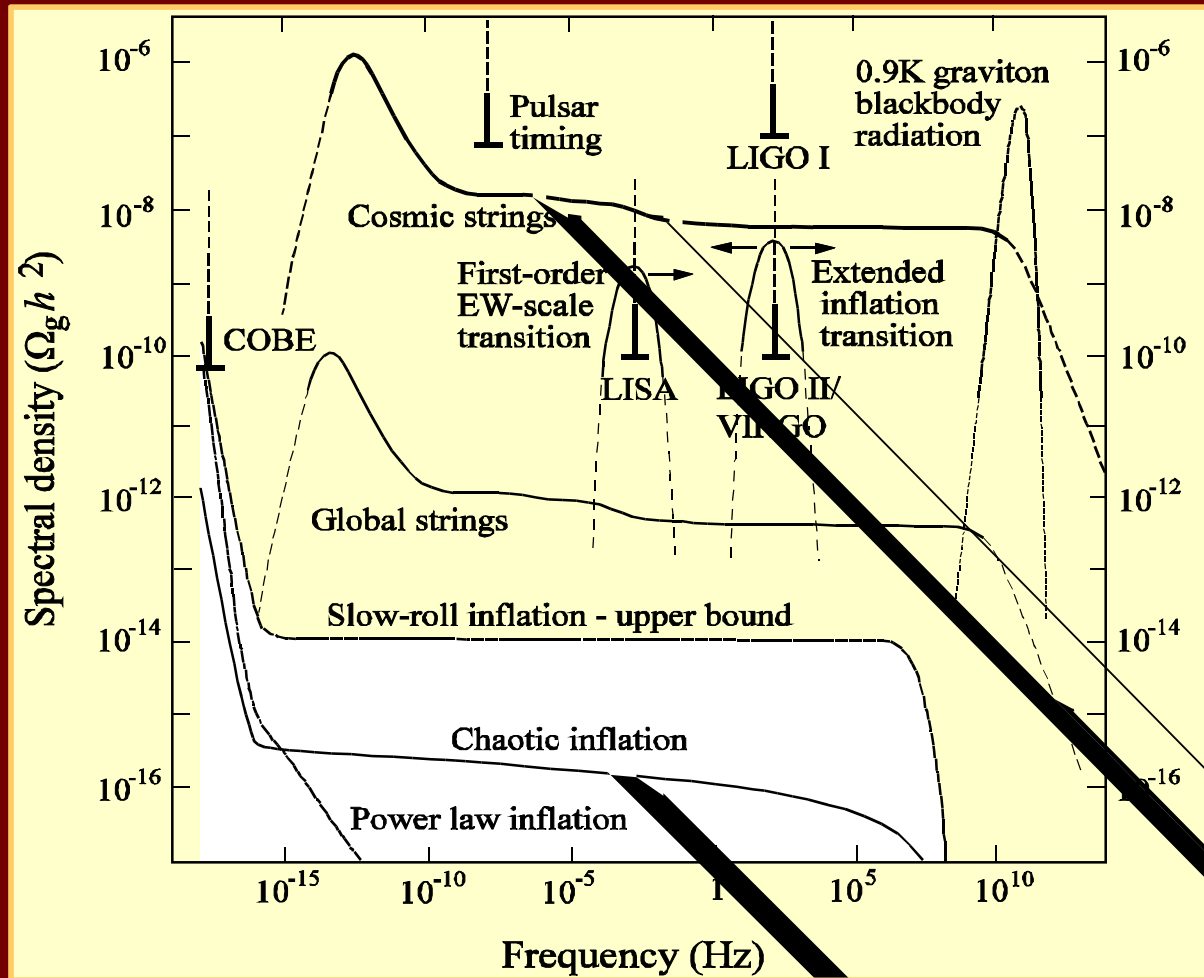


THE GRAVITATIONAL WAVE SPECTRUM



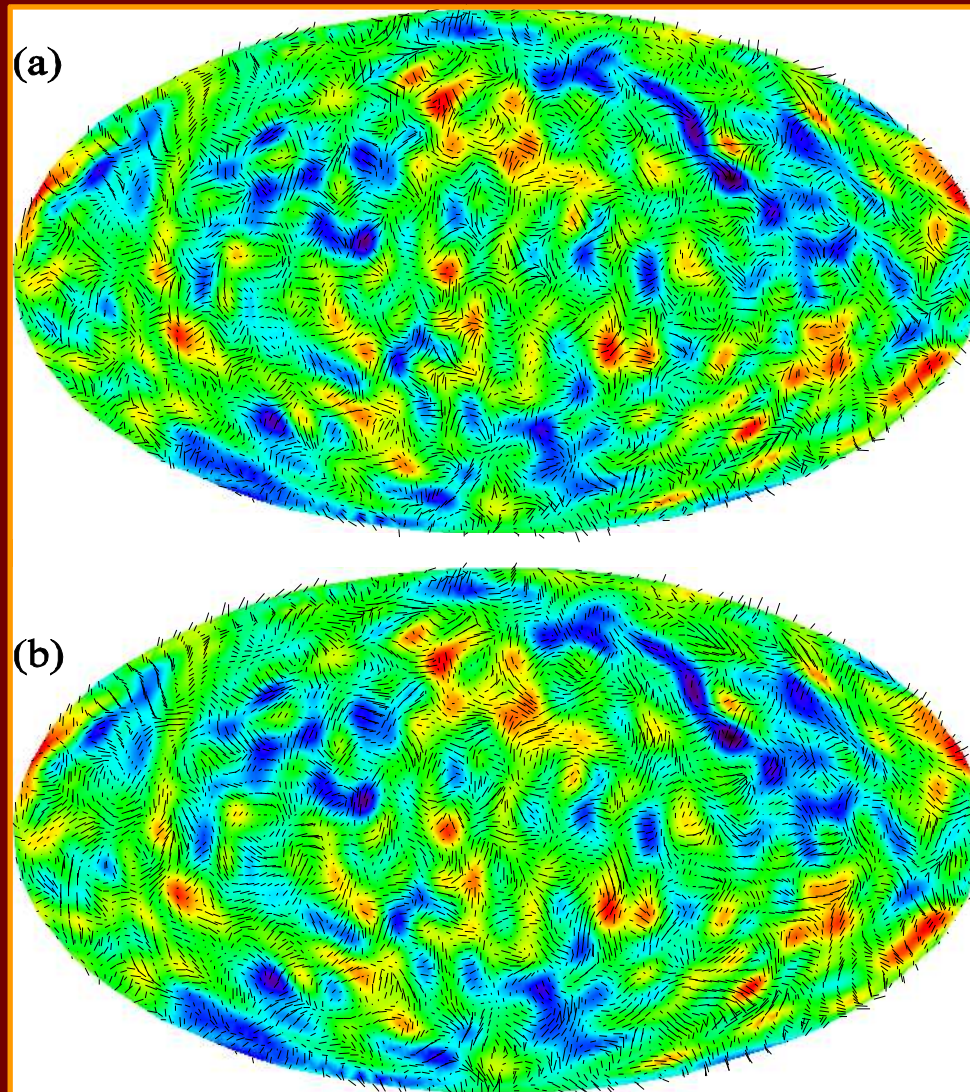
LISA (~2012;
test flight next year)

The search for primordial gravitational waves



Detecting GW via “B-mode” CMB polarization

a) Pure scalar (E) modes



b) Pure tensor (B) modes

Caldwell et al. 1998

Gravity waves: the “smoking gun” of inflation

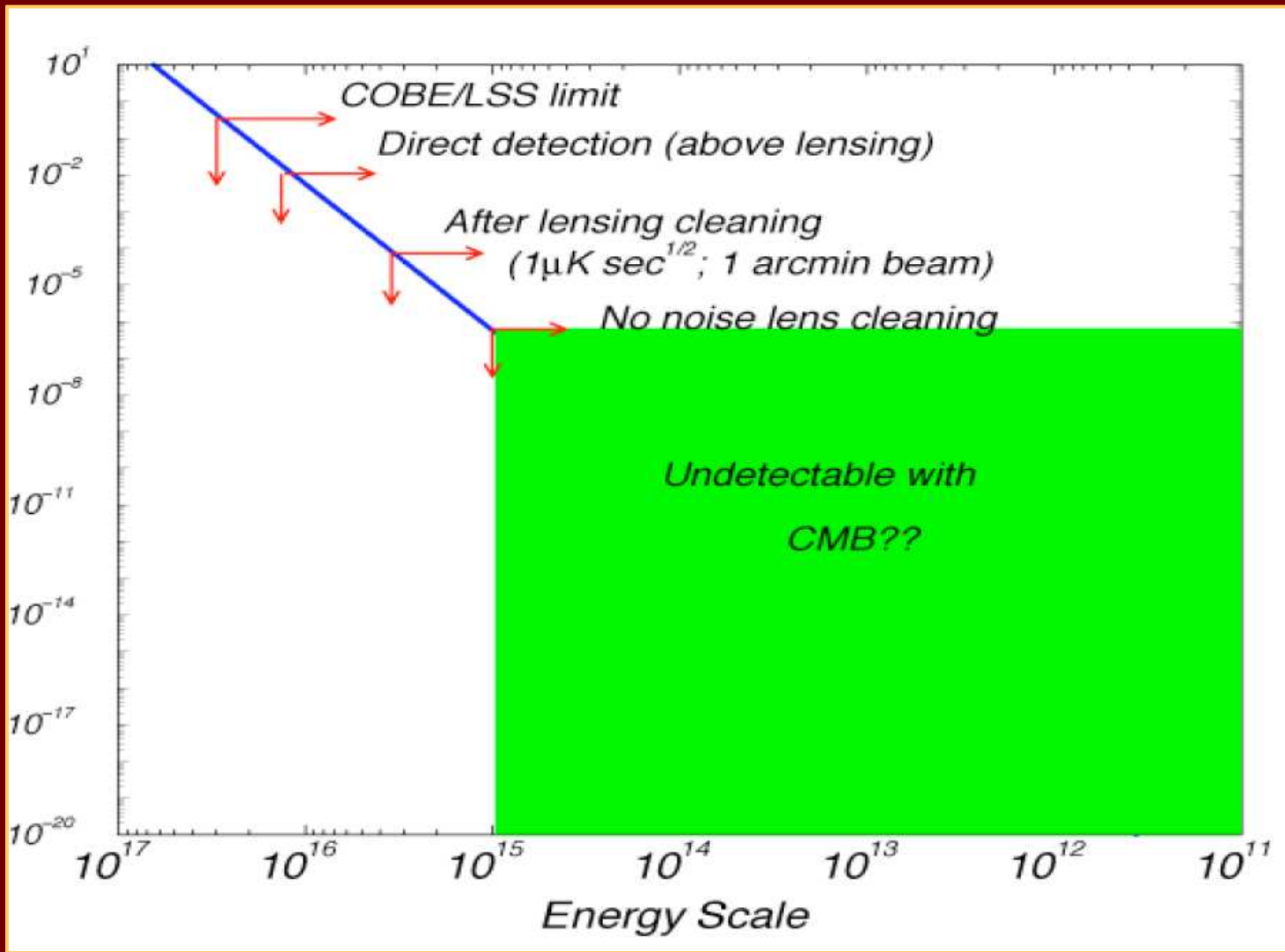
The spectra $P_R(k)$ and $P_T(k)$ provide the contact between theory and observations. The *WMAP* (+SDSS) dataset allows to extract an upper bound, $r < 0.28$ (95% CL) (Spergel 2006), or $\varepsilon < 0.017$. This limit provides an upper bound on the energy scale of inflation

$$V^{1/4} < 2.6 \times 10^{16} \text{ GeV}$$

5. A positive detection of the B-mode in CMB polarization, and therefore an indirect evidence of gravitational waves from inflation, once foregrounds due to gravitational lensing from local sources has been properly treated, requires $\varepsilon < 10^{-5}$, corresponding to

$$V^{1/4} > 3.5 \times 10^{15} \text{ GeV}$$

Tensor-to-scalar ratio



Cooray 2004

Detectability of IGB

2510 A. Cooray

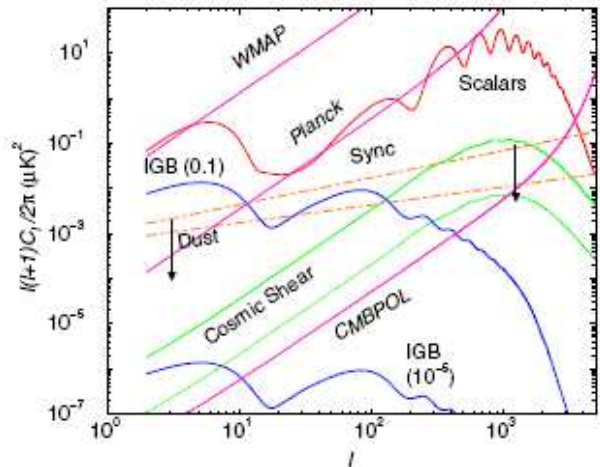


Fig. 2. CMB polarization anisotropies in the gradient (E) mode due to scalars and curl (B) modes due to the inflationary gravitational wave background (curve labeled “IGB”, with the number in parenthesis showing the normalization in terms of the tensor-to-scalar ratio, which in terms of the energy scale of inflation is 2×10^{16} GeV (0.1), top curve, and 2×10^{15} GeV (10^{-5}), bottom curve). Note the effect due to reionization where rescattering produces new large angular scale anisotropies. For optical depths at the level of 0.1, the peak of the power related to IGW curl modes is at tens of degree angular scales and not at the degree scale ($\ell \sim 100$) corresponding to the bump at recombination. Note that this enhancement, amounting to over two magnitudes in power at $\ell \sim$ few is significant and aid potential detectability of the IGWs via polarization. The IGW detection is confused with cosmic shear conversion of a fractional E-mode \rightarrow B-mode by the intervening large scale structure. The residual noise curve related to cosmic shear is after doing lens-cleaning in polarization maps with an arcminute scale CMB experiment with instrumental polarization sensitivity at the level of $1 \mu\text{K}\sqrt{\text{sec}}$. For reference, we show an estimated level of contamination from dust and synchrotron emission (at 150 GHz); this noise level can be improved with foreground cleaning in multifrequency data with sensitivity better than the foreground noise contributions. The curve labeled Planck is the noise curve related to upcoming Planck (HFI) polarization observations as a function of each multipole.

2516 A. Cooray

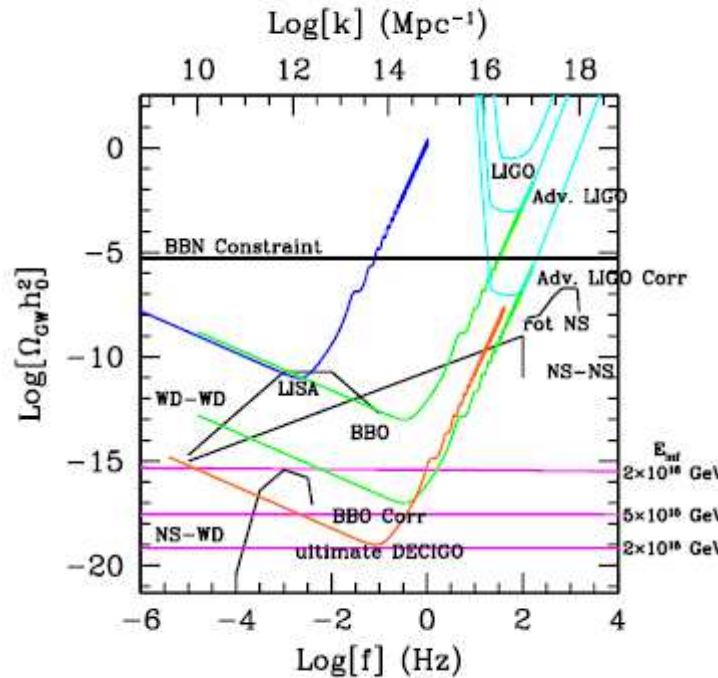


Fig. 5. Same as Fig. 4, but we show the background at frequencies related to the proposed Big Bang Observer mission. For comparison, we also show the expected stochastic backgrounds from foreground sources such as neutron star-neutron star binaries (e.g., Ref. 54), white dwarf-white dwarf binaries (e.g., Ref. 16), neutron star-white dwarf binaries (e.g., Ref. 10), and the background related to single rotational neutron stars.¹⁷ For a reliable detection of the inflationary gravitational wave signal, the background related to neutron stars must be removed. This can be achieved given the low merger rate of these binaries and the rapid orbital evolution of the binary such that the gravitational wave frequency across this band changes substantially over the observational period.

Detectability of IGB (direct + indirect)

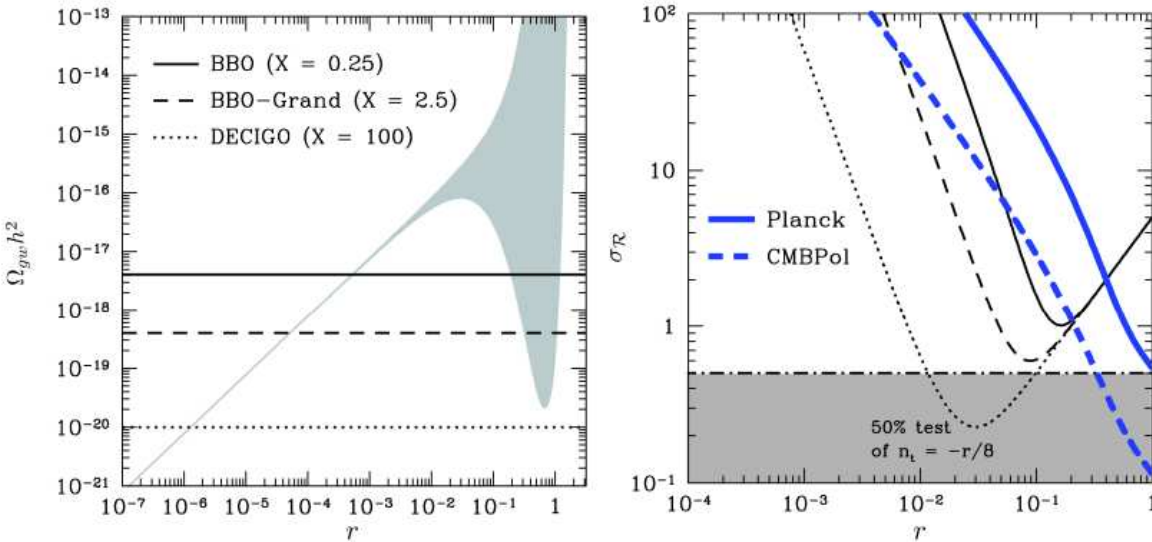
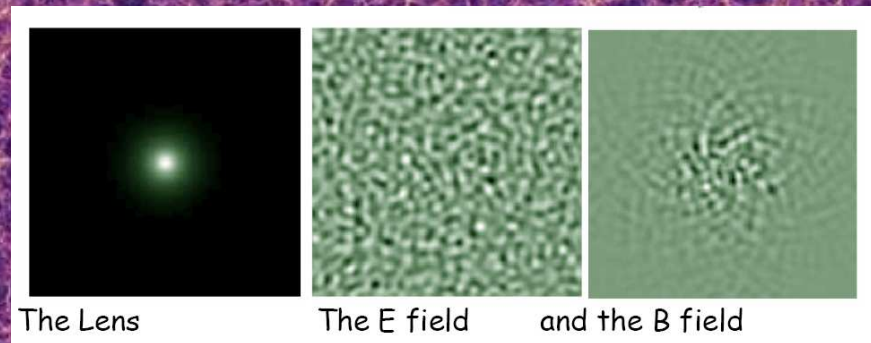


FIG. 2: *Left:* The mapping between tensor-to-scalar ratio r at CMB scales and $\Omega_{\text{GW}} h^2$ at 1 Hz for a direct detection. The gray shaded region shows the uncertainty implied with $n_s = 0.95 \pm 0.1$ [19] by keeping terms up to second order (running of the tensor spectral index) in the slow-roll power-law expansion. The three horizontal curves are the 2σ detection amplitudes for BBO-standard , BBO-grand, and DECIGO in solid, dashed, and dotted lines respectively. In these three experiments, at 1 Hz, the signal-to-noise ratio for detecting the gravitational wave background is $\text{SNR} = X(\Omega_{\text{GW}}/10^{-18})$, with values for X shown in the panel. *Right:* The 1σ uncertainty in the single-field consistency relation $\mathcal{R} \equiv -r/8n_t$. The thin lines follow laser interferometers in the right panel, showing the error expected by combining direct detection measurements of n_t with CMBPol measurements of the tensor-to-scalar ratio, r . The two thick lines indicate errors in \mathcal{R} when n_t is determined from CMB alone. The thick solid curve corresponds to the expected accuracy of ESA's Planck satellite, the thick dashed curve corresponds to CMBPol. The shaded region indicates a 50% determination of the consistency relation ($\mathcal{R} = 1.0 \pm 0.5$). For direct-detection observations, sensitivity is degraded at large r because of an increase in the uncertainty of the running of the tensor spectral index from direct detection scales to CMB scales; at small r , the accuracy with which \mathcal{R} can be determined is dominated by the error in measuring n_t with CMB [20] and laser interferometers [11], where the latter is $\sigma_{n_t} \propto 1/r$.

1 Gpc/h

Millennium Simulation

10.077.696.000 particles



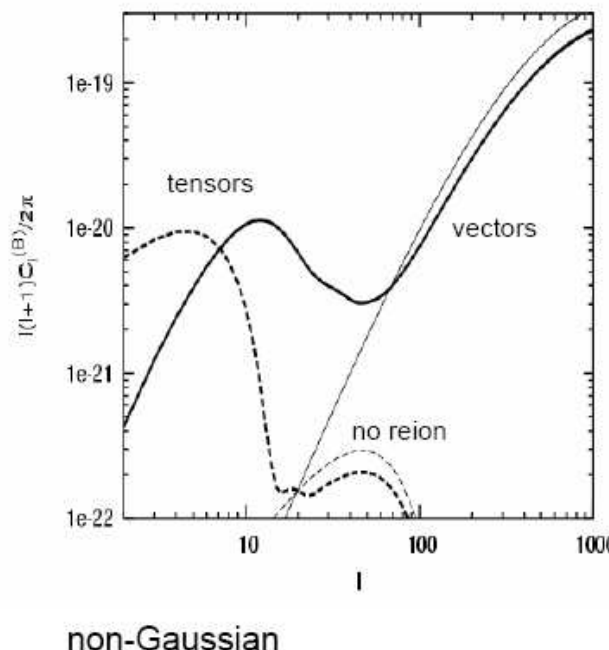
CMB Millennium Lensing (Carbone, Baccigalupi, Matarrese, Springel, White et al. in preparation: produce simulated temperature and (E and B mode) CMB polarization maps lensed by the DM structures
 $(z = 0)$

Secondary effects vs. IGB

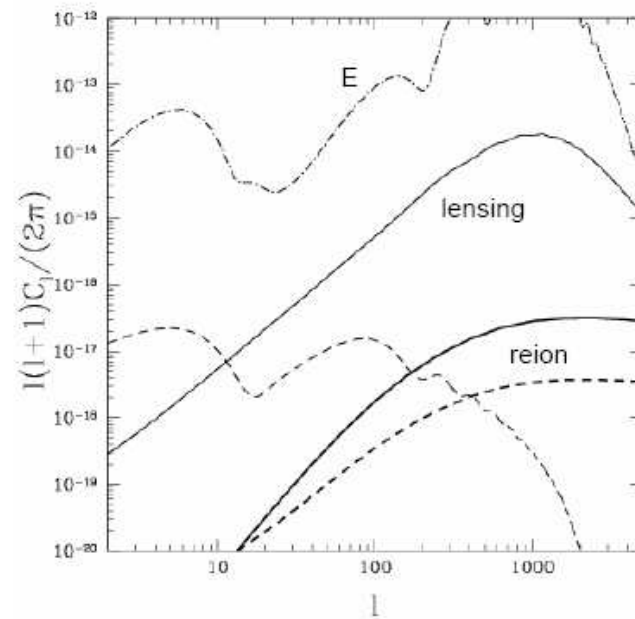
The B-mode polarization produced by primordial gravitational waves can be hidden by gravitational lensing and/or by second-order vector and tensor modes, unless the inflation energy scale is larger than 10^{15} GeV. Our ability of delensing polarization maps is the crucial issue in this problem (e.g. Hirata & Seljak 2004; Sigurdson & Cooray 2005).

- Small second order effects, e.g.

Second order vectors and tensors:
Mollerach, Harari, Matarrese: [astro-ph/0310711](#)



Inhomogeneous reionization
Santon, Cooray, Haiman, Knox, Ma:
[astro-ph/0305471](#); Hu: [astro-ph/9907103](#)



GW from non-linear cosmological perturbations

$$h^{\alpha}_{\beta}(\eta, \mathbf{x}) = \frac{4G}{c^4} \frac{1}{ar} \mathcal{P}^{\alpha}_{\nu} \mathcal{R}^{\nu}_{\beta} \left[a^3 \int d^3 \tilde{x} \mathcal{R}_{\text{eff}}^{\nu} \right]_{\text{ret}}$$

$$\begin{aligned} \mathcal{R}_{\text{eff}}^{\alpha}_{\beta} &= \rho \left(v^{\alpha} v_{\beta} - \frac{1}{3} v^2 \delta^{\alpha}_{\beta} \right) + \\ &+ \frac{1}{4\pi G a^2} \left(\partial^{\alpha} \varphi \partial_{\beta} \varphi - \frac{1}{3} \partial^{\nu} \varphi \partial_{\nu} \varphi \delta^{\alpha}_{\beta} \right) \end{aligned}$$

Carbone & Matarrese 2005

tensor-mode projection operator

Tensor (and vector!) metric modes are generated by scalar (e.g. density) perturbations as soon as the latter become non-linear. As a result GW are produced during the later stages of cosmological structure formation with typical period of the order of the Hubble time.

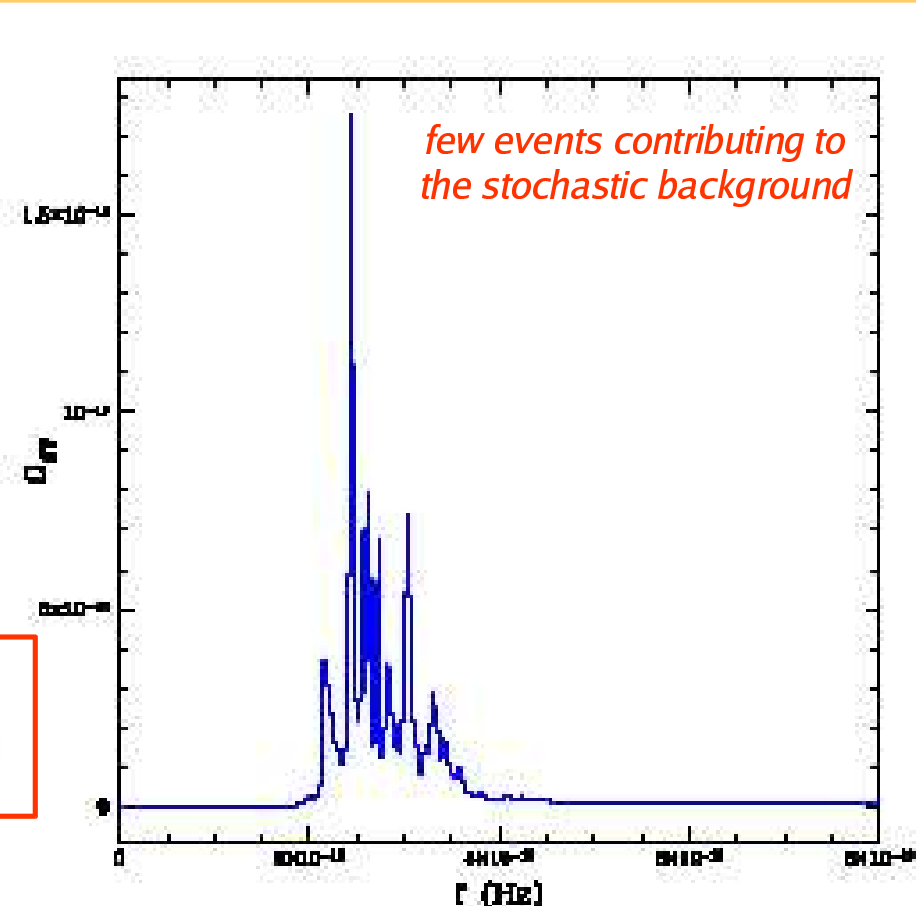
GW from the collapse of DM halos

During the formation of non-spherical DM halos low-frequency GW are emitted, thus forming a stochastic background with amplitude comparable with the primordial one for an inflation energy scale $\sim \text{few} \times 10^{15} \text{ GeV}$.

The typical GW strain amplitude for a non-spherical halo of mass M and size L at a distance D is

$$h \approx \frac{3 \times 10^{-11}}{D/100\text{Mpc}} \times \frac{GM (10^{15})^{2/7}}{c^2 L} \times \frac{M}{10^{15} M_\odot},$$

This also produces CMB temperature anisotropy and polarization by secondary effects

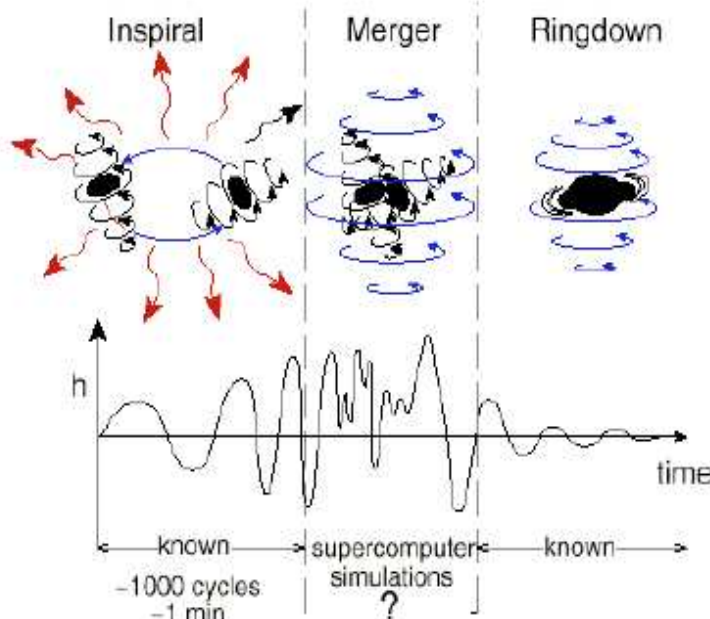


Carbone, Baccigalupi & Matarrese 2005

GW from Black-Hole Binaries

Binary Black Holes as a Tool in Astronomy

- The inspiral phase
 - well described by post-Newtonian
 - well defined parameters including masses, spins and orbits of initial holes.
- The merger phase
 - highly nonlinear dynamics of curved spacetime
 - expensive numerical calculations
- The ringdown phase
 - exponentially damped sinusoid
 - includes information about the mass and spin of the final black hole.



GW from MBHB

Low-frequency gravitational radiation from coalescing massive black holes

A Sesana¹, F Haardt¹, P Madau² and M Volonteri²

¹ Dipartimento di Fisica e Matematica, Università dell'Insubria, via Valleggio 11, 22100 Como, Italy

² Department of Astronomy and Astrophysics, University of California, 1156 High Street, Santa Cruz, CA 95064, USA

Received 29 October 2004, in final form 17 January 2005

Published 26 April 2005

Online at stacks.iop.org/CQG/22/S363

Abstract

We compute the expected low-frequency gravitational wave signal from coalescing massive black-hole (MBH) binaries at the centres of galaxies. We follow the merging history of halos and associated holes via cosmological Monte Carlo realizations of the merger hierarchy from early times to the present in a Λ CDM cosmology. MBHs get incorporated through a series of mergers into larger and larger halos, sink to the centre owing to dynamical friction, accrete a fraction of the gas in the merger remnant to become more massive, and form a binary system. Stellar dynamical processes dominate the orbital evolution of the binary at large separations, while gravitational wave emission takes over at small radii, causing the final coalescence of the system. We discuss the observability of inspiralling MBH binaries by a low-frequency gravitational wave experiment such as the planned Laser Interferometer Space Antenna (LISA), discriminating between resolvable sources and unresolved confusion noise. Over a three-year observing period LISA should resolve this GWB into discrete sources, detecting ≈ 90 individual events above a $S/N = 5$ confidence level, while expected confusion noise is well below planned LISA capabilities.

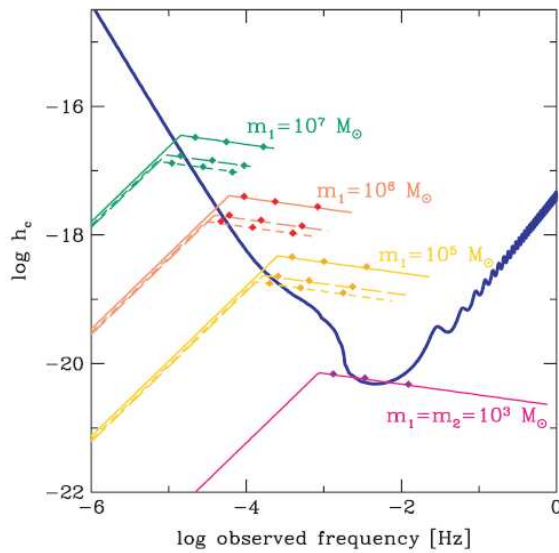


Figure 2. Characteristic strain spectrum h_c against frequency: from top to bottom, the three sets of curves refer to systems with $\log(m_1/M_\odot) = 7, 6, 5$ respectively, and the solid, long-dashed, and short-dashed lines assume the binary at $z = 1, 3, 5$ respectively. A mass ratio $m_2/m_1 = 0.1$ is assumed. The lowest curve is for an equal mass binary $m_1 = m_2 = 10^3 M_\odot$ at $z = 7$. The small diamonds on each curve mark, from left to right, the frequency 1 year, 1 month and 1 day before coalescence. Thick solid curve: LISA sensitivity threshold approximately accounting for detection with $S/N > 5$ including galactic [9] and extragalactic [10] white dwarf binary (WD-WD) confusion noises (added in quadrature). A three-year observation is considered.

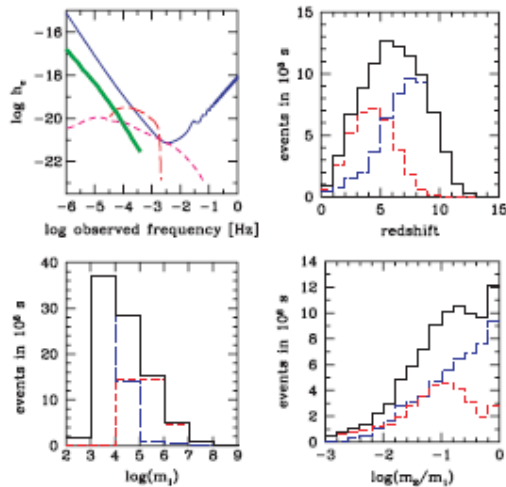


Figure 4. Upper left panel: confusion noise due to MBHBs as a function of frequency (thick solid line). Other lines have the same meaning as in figure 3, left panel. Upper right panel: differential redshift distribution of MBHBs resolved with $S/N > 5$ by LISA in a three-year mission (solid lines). The separate counts for MBs (short-dashed line) and IBs (long-dashed line) are also shown. Lower left panel: mass distribution of the more massive members of MBHBs; line style as in the right upper panel. Lower right panel: mass ratio distribution of MBHBs; line style as in the right upper panel.

The present-day view on non-Gaussianity

Alternative structure formation models of the eighties considered strongly non-Gaussian primordial fluctuations.

- 3. The increased accuracy in CMB and LSS observations has, however, excluded this extreme possibility.
- 5. The present-day challenge is to either detect or constrain mild or even weak deviations from primordial Gaussianity.
- 7. Deviations of this type are not only possible but are unavoidably predicted in the standard perturbation generating mechanism provided by inflation.

Inflationary non-Gaussianity

Many primordial (inflationary) models of non-Gaussianity can be represented in configuration space by the general formula (e.g. Verde *et al.* 2000; Komatsu & Spergel 2001)

3.

$$\Phi = \phi_L + f_{NL} * (\phi_L^2 - \langle \phi_L^2 \rangle)$$

5. where Φ is the large-scale gravitational potential, ϕ_L its linear Gaussian contribution and f_{NL} is the dimensionless non-linearity parameter (or more generally non-linearity function). The percent of non-Gaussianity in CMB data implied by this model is

6.

7.

$$\text{NG \%} \sim 10^{-5} |f_{NL}|$$

< 10^{-3} from
WMAP

Where does large-scale non-Gaussianity come from?

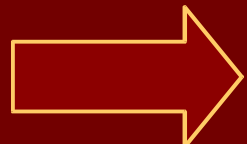
¶ *Falk et al. (1993)* found $f_{\text{NL}} \sim \xi \sim \epsilon^2$ (from non-linearity in the inflaton potential in a fixed de Sitter space) in the standard single-field slow-roll scenario

¶ *Gangui et al. (1994)*, using stochastic inflation found $f_{\text{NL}} \sim \epsilon$ (from second-order gravitational corrections during inflation).

Acquaviva, Bartolo, Matarrese & Riotto (2003) and *Maldacena (2003)* confirmed this estimate (up to numerical factors and momentum-dependent terms) with a full second-order approach

¶ *Bartolo et al. (2004)* show that second-order corrections after inflation enhance the primordial signal leading to $f_{\text{NL}} \sim 1$

Non-Gaussianity requires more than linear theory ...



The leading contribution to higher-order statistics (such as the bispectrum, i.e. the FT of the three-point function) comes from second-order metric perturbations around the RW background (unless the primordial non-Gaussianity is very strong)

“... the linear perturbations are so surprisingly simple that a perturbation analysis accurate to second order may be feasible ...”

Sachs & Wolfe 1967

Non-Gaussianity from Inflation: results

The amount of non-Gaussianity from a wide class of models, including single-field slow-roll inflation, curvaton (*Mollerach 1990; Moroi & Takahashi 2001; Enqvist & Sloth 2002; Lyth & Wands 2002*) and modulated reheating (*Hamazaki & Kodama 1996; Dvali et al. 2003; Zaldarriaga 2003; Kofman 2003*), follows a universal (second-order) relation:

$$\Delta T/T = \frac{1}{3} (\phi_L + \phi_{NL})$$

$\phi_{NL} = f_{NL} * \phi_L^2 + const.$

$f_{NL} = f_{NL}^0 - 3(k_1^4 + k_2^4)/2k^4 - (k_1 \cdot k_2 / k^2) \cdot$
 $\cdot [4 - 3(k_1 \cdot k_2 / k^2)]$

Sachs-Wolfe limit; replaced by full transfer function in CMB maps

Predicted values of f_{NL}

	$f_{NL}(\mathbf{k}_1, \mathbf{k}_2)$	Comments
Single-field inflation	$\frac{4}{3} - g(\mathbf{k}_1, \mathbf{k}_2)$	$g(\mathbf{k}_1, \mathbf{k}_2) = 4\frac{\mathbf{k}_1 \cdot \mathbf{k}_2}{k^2} - 3\frac{(\mathbf{k}_1 \cdot \mathbf{k}_2)^2}{k^4} + \frac{3}{2}\frac{k_1^4 + k_2^4}{k^4}$
Curvaton scenario	$\left[-\frac{1}{3} - \frac{5}{6}r + \frac{5}{4r}\right] - g(\mathbf{k}_1, \mathbf{k}_2)$	$r \approx \left(\frac{\rho_\sigma}{\rho}\right)_{decay}$
Inhomogeneous reheating	$\frac{1}{12} - I - g(\mathbf{k}_1, \mathbf{k}_2)$	$I = -\frac{5}{2} + \frac{5}{12}\frac{\bar{\Gamma}}{\alpha\Gamma_1}$ “minimal case” $I = 0$ ($\alpha = \frac{1}{6}$, $\Gamma_1 = \bar{\Gamma}$)
Multiple scalar fields	$\frac{\mathcal{P}_S}{\mathcal{P}_R} \cos^2 \Delta \left(4 \cdot 10^3 \cdot \frac{V_{xx}}{3H^2}\right) \cdot 60 \frac{H}{\chi}$	order of magnitude estimate of the absolute value
“Unconventional” inflation set-ups		
Warm inflation	$-\frac{5}{6} \left(\frac{\dot{\varphi}_0}{H^2}\right) \left[\ln\left(\frac{\Gamma}{H}\right) \frac{V'''}{\Gamma}\right]$	second-order corrections not included
Ghost inflation	$-85 \cdot \beta \cdot \alpha^{-8/5}$	post-inflationary corrections not included
D-deceleration	$-0.06 \gamma^2$	post-inflationary corrections not included

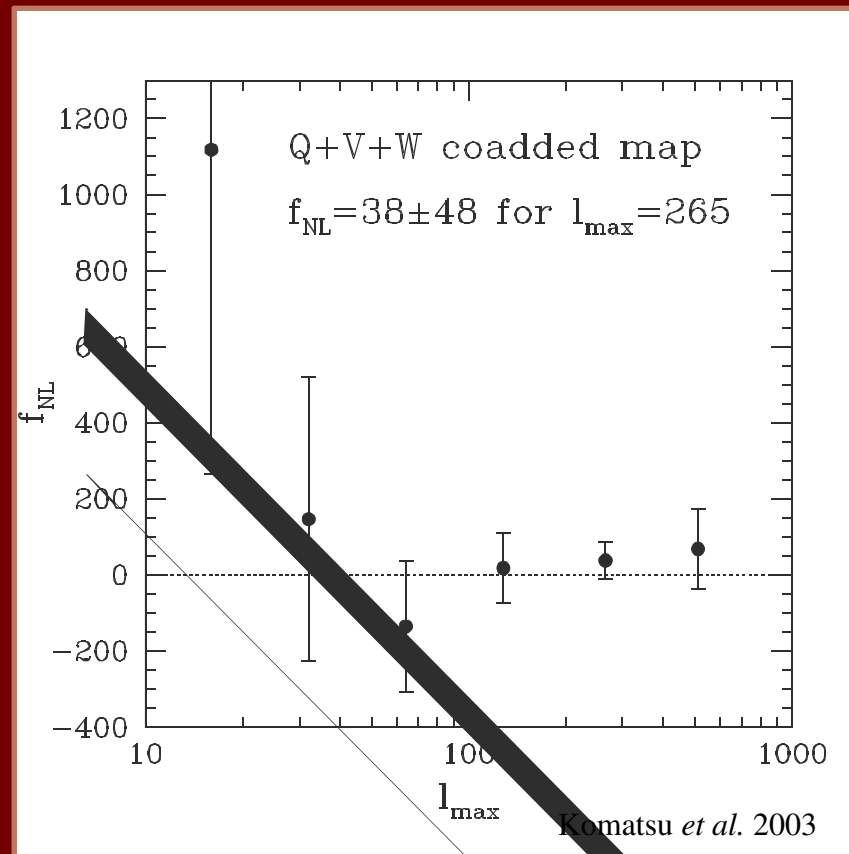
In the region $f_{NL} \sim 1$ second-order corrections are significant. Important to control the different NG generated in the various stages of the perturbation evolution to fully exploit CMB data 61

Observational constraints on f_{NL}

The strongest limits on non-Gaussianity comes from 3-yr WMAP data. *Spergel et al. (2006)* find (95% CL):

$$-54 < f_{NL} < 114$$

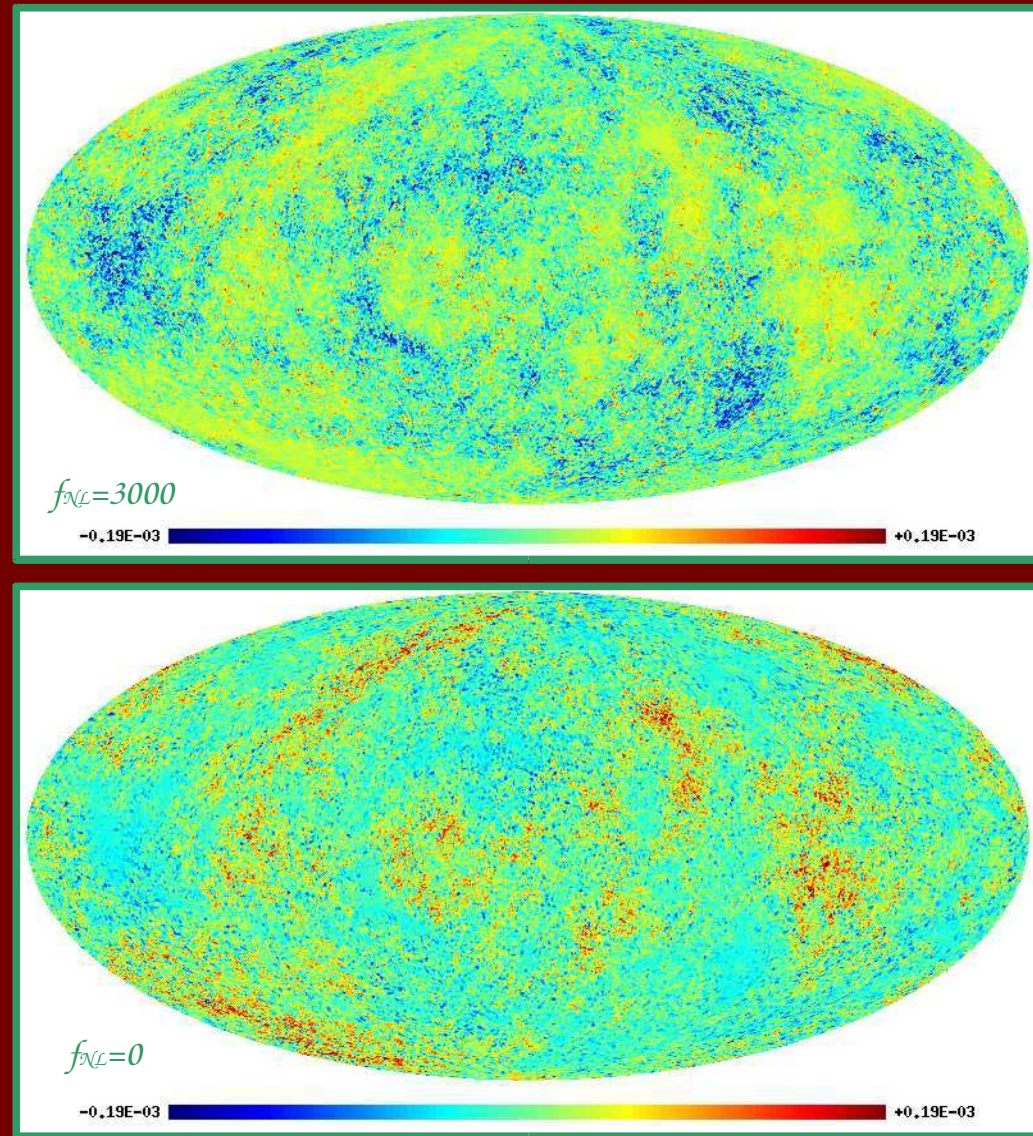
4. According to *Komatsu & Spergel (2001)* using the angular bispectrum one can reach values as low as $|f_{NL}| = 20$ with *WMAP* & $|f_{NL}| = 5$ with *Planck* can be achieved
8. The role of the f_{NL} momentum-dependent is a characteristic inflation signature that can enhance the S/N for NG detection (*Liguori, Hansen, Komatsu, Matarrese & Riotto 2005*), possibly making single-field inflation NG detectable



Gaussian vs. non-Gaussian

The *WMAP* data put a limit on the non-Gaussianity strength parameter f_{NL} (*Komatsu et al. 2003; Spergel et al. 2006*; see also *Creminelli et al. 2005*, for equilateral configurations; *Liguori, Hansen, Komatsu, Matarrese & Riotto 2005*, for full account of shape-dependence)

$$-54 < f_{\text{NL}} < 114$$



Simulated maps of CMB anisotropies expected in a Λ CDM model. Upper panel: a simulated *PLANCK* map with non-Gaussian potential fluctuations. Lower panel: the same realization of the sky with Gaussian potential fluctuations *PLANCK* (*Liguori, Matarrese & Moscardini 2003*). Few hundred simulated maps at the Planck resolution have been produced for arbitrary f_{NL}

Searching for non-Gaussianity with rare events

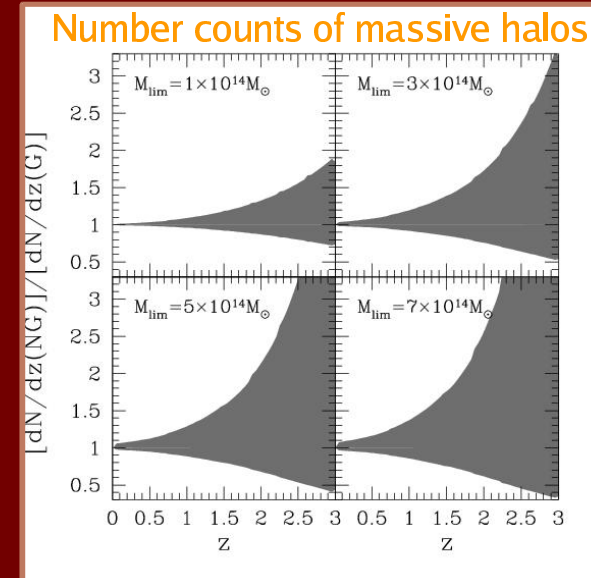
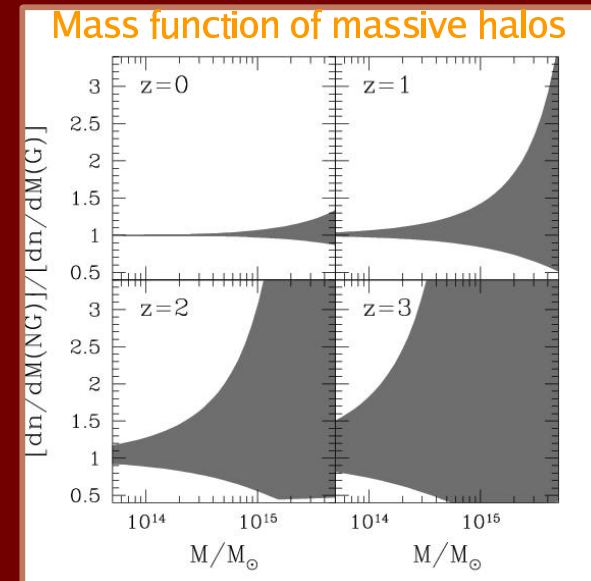
Besides using standard statistical estimators, like bispectrum, trispectrum, three and four-point function, skewness , etc. ..., one can look at the tails of the distribution, i.e. at rare events.

3. Rare events have the advantage that they often maximize deviations from what predicted by a Gaussian distribution, but have the obvious disadvantage of being ... rare!
5. Matarrese, Verde & Jimenez (2000) and Verde, Jimenez, Kamionkowski & Matarrese have shown that clusters at high redshift ($z>1$) can probe NG down to $f_{NL} \sim 10^2$ which is, however, not competitive with future CMB (Planck) constraints

Wednesday, October 11, 2000

FPS-06 Frascati

Komatsu et al. 2003



Searching for non-Gaussianity with LSS

Verde et al. (1999) and Scoccimarro et al. (2004) showed that constraints on primordial non-Gaussianity in the gravitational potential from large redshift-surveys like 2dF and SDSS are not competitive with CMB ones: f_{NL} has to be larger than $10^2 - 10^3$ in order to be detected as a sort of non-linear bias in the galaxy-to-dark matter density relation. However LSS gives complementary constraints, as it probes NG on different scales than CMB. Hint: use reconstruction of initial data (e.g. Mohayaee et al. 2004) to detect primordial NG.

Going to redshift $z \sim 1$ helps (but one would need surveys covering a large fraction of the sky). Scoccimarro et al. (2004) claim that a bispectrum analysis over a hypothetical all-sky survey at $z \sim 1$ might detect NG down to $f_{NL} \sim 1$ (quite likely too optimistic because of the large wave-number range used in the estimate). Going to high redshift (e.g. through the 21-cm background anisotropies largely helps, as the effective NG strength in the underlying CDM overdensity scales like $(1+z)$ (Matarrese, Pillepich & Porciani, in prep.).

5. Primordial non-Gaussianity also strongly affects the abundance of the first non-linear objects in the Universe, thereby modifying the reionization epoch (Chen et al. 2003) Is a large result z_{reion} such as 20-30 more likely?

N-body simulations of NG models

Branchini, Dolag, Grossi, Matarrese, Moscardini, 2006, in preparation

- 3. **800³ particles**, corresponding to a mass-resolution of $m_p \approx 2 * 10^{10}$ solar masses
- 5. Cosmological boxes: **L=500³ (Mpc/h)³**
- 7. Computations performed at CINECA Supercomputing Centre (Bologna) on a3k (only initial conditions) and sp5 machines: about 7000 hours of CPU time per simulation.

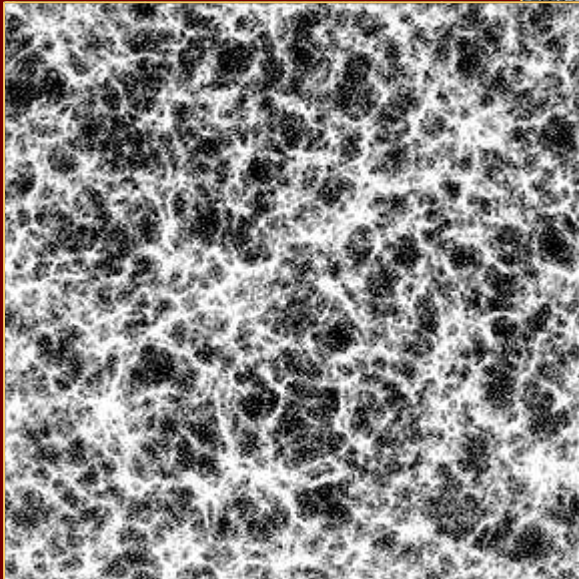
10 Mpc/h

Slices

z = 3.1

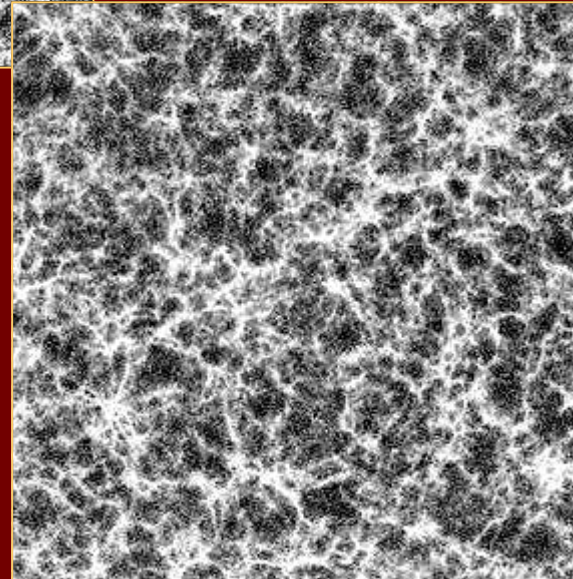
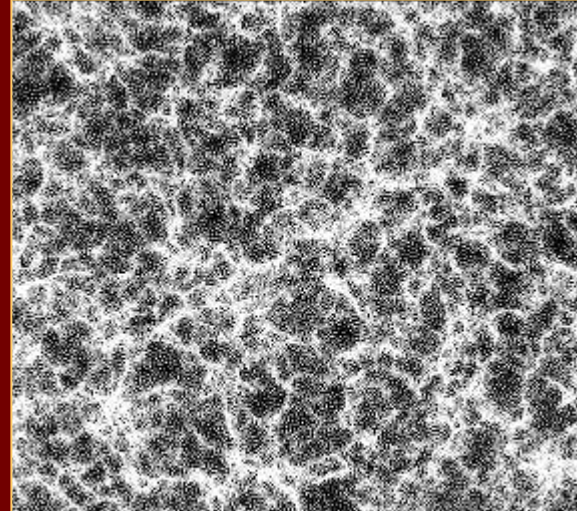
$f_{\text{NL}} = 0$

Gaussian model



$f_{\text{NL}} = -2000$

Wednesday, October 11, 200



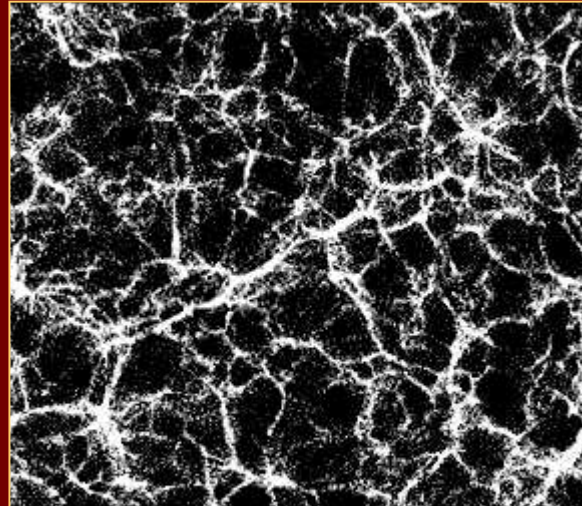
$f_{\text{NL}} = +2000$

FPS-06 Frascati

67

10 Mpc/h

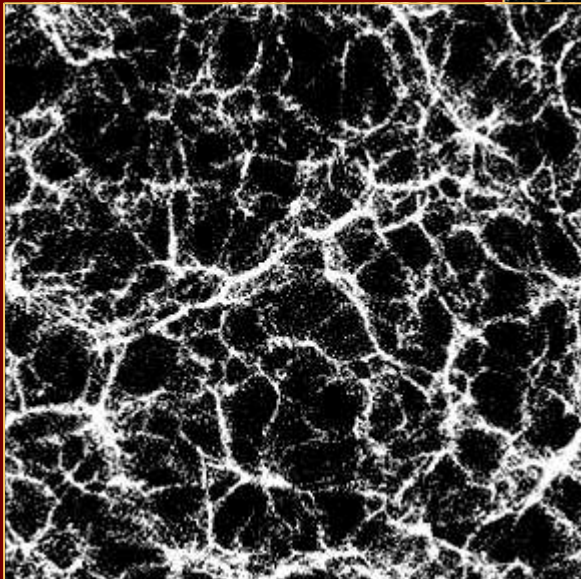
Slices



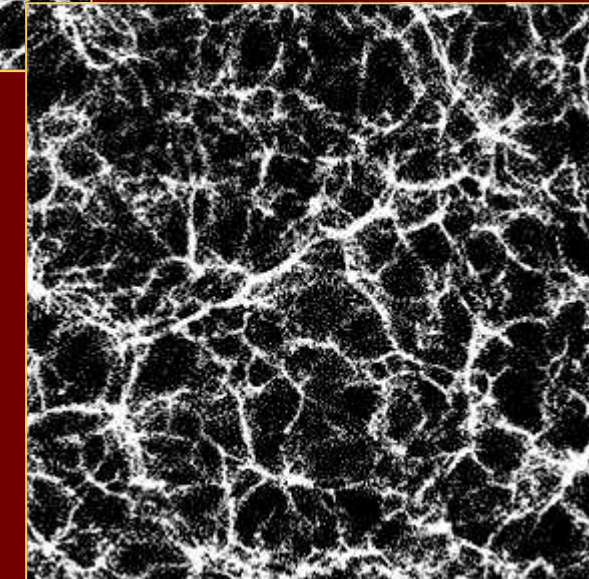
z = 0.

$$f_{\text{NL}} = 0$$

Gaussian model

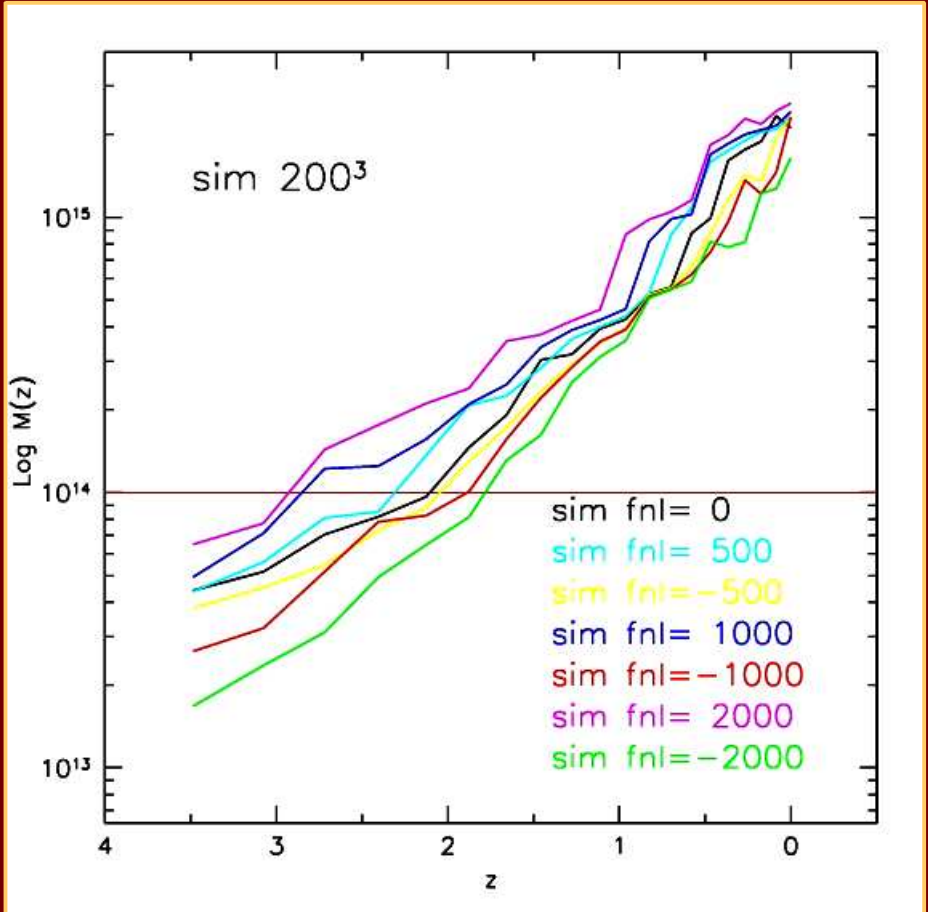


$$f_{\text{NL}} = -2000$$



$$f_{\text{NL}} = +2000$$

Rare event statistics: the redshift evolution of the mass of the largest object



The formation time :

it can change

up to one in Δz !

Cosmic Magnetic Fields

Harrison's (1970) mechanism for magnetic seed generation in the early Universe

Consider a rotating region in the expanding early Universe (with scale factor a), consisting of matter (mostly protons) with average energy density ρ_m , electrons and photons with energy density ρ_γ . Electrons and photons are tightly coupled and are considered as a single fluid in Ref. [10]. Let ω_m and ω_γ be their angular velocities. In the absence of interactions, their angular momenta, proportional, respectively, to $\rho_m \omega_m a^5$, and $\rho_\gamma \omega_\gamma a^5$, are separately conserved (see also the Appendix). As the Universe expands, they scale differently, $\omega_m \propto a^{-2}$ and $\omega_\gamma \propto a^{-1}$. Ions and the electron-photon fluid spin down at different rates and then currents and magnetic fields are generated.

but ... Kelvin's circulation theorem prevents the occurrence of vorticity in the primordial plasma, unless it was there in the initial (post-inflationary) conditions which is not the case in standard scenarios

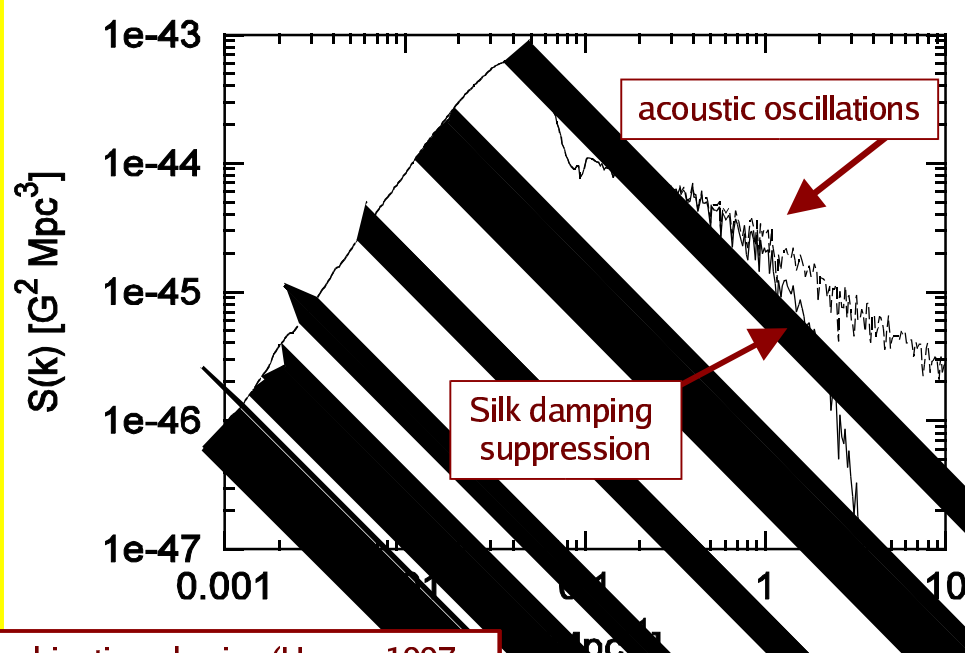
Magnetic field generation from secondary vector modes

Matarrese, Mollerach, Notari & Riotto 2005, Phys. Rev. D71, 043502

We derive the *minimal* seed magnetic field which unavoidably arises in the radiation and matter eras, prior to recombination, by the rotational velocity of ions and electrons, gravitationally induced by the non-linear evolution of primordial density perturbations. The resulting magnetic field power-spectrum is fully determined by the amplitude and spectral index of density perturbations. The *rms* amplitude of the seed-field at recombination is $B \approx 10^{-23}(\lambda/\text{Mpc})^{-2}$ G, on comoving scales $\lambda \gtrsim 1$ Mpc.

While the total vorticity of the system is conserved – in full agreement with Kelvin's circulation theorem – and can be set to zero, electrons and protons acquire a non-zero rotational velocity from the second-order metric vector mode, which in turn arises from the mode-mode coupling of primordial scalar modes. This rotational velocity gives rise to a seed magnetic field, according to Harrison's mechanism.

$$B(\mathbf{k}, \eta) = -\frac{m_p(1+z)}{e\mathcal{H}^2} \int \frac{d^3 k'}{(2\pi)^3} \mathbf{k} \times \mathbf{k}' \\ \left[2\varphi'(|\mathbf{k} - \mathbf{k}'|)\varphi(k') - \frac{k'^2}{12\mathcal{H}^2}\varphi'(|\mathbf{k} - \mathbf{k}'|)\varphi(k') \right. \\ \left. - \frac{k'^2}{12\mathcal{H}}\varphi(|\mathbf{k} - \mathbf{k}'|)\varphi(k') \right],$$



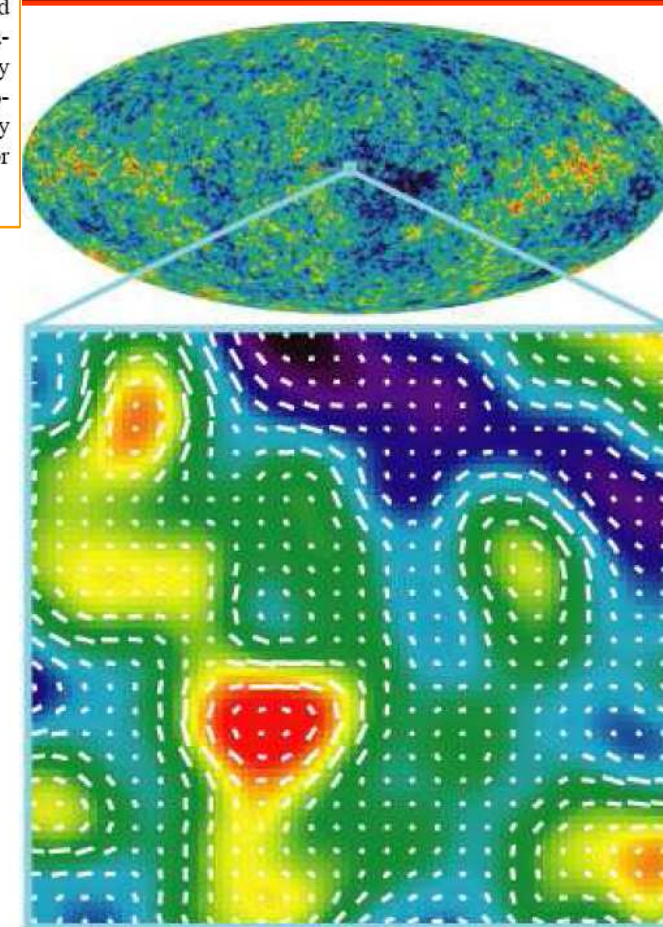
Note: magnetic field generation will also arise due to recombination physics (Hogan 1997; Dolgov & Berezhiani 2003) and reionization (Aghanim et al. 2001; Gnedin et al. 2001); Takahashi et al. (2005) claim a 6 order of magnitude larger effect from the collision term.

Cosmic Magnetic Fields from Density Perturbations

Abstract. We discuss generation of magnetic field from cosmological perturbations. We consider the evolution of three component plasma (electron, proton and photon) evaluating the collision term between electrons and photons up to the second order. The collision term is shown to induce electric current, which then generate magnetic field. There are three contributions, two of which can be evaluated from the first-order quantities, while the other one is fluid vorticity which is purely second order. We compute numerically the magnitudes of the former contributions and shows that the amplitude of the produced magnetic field is about $\sim 10^{-19}$ G at 10kpc comoving scale at present. Compared to astrophysical and inflationary mechanisms for seed-field generation, our study suffers from much less ambiguities concerning unknown physics and/or processes.

Takahashi et al. 2006

Fig. 1. All sky map of cosmological microwave background anisotropy obtained by the Wilkinson Microwave Anisotropy Probe (WMAP) satellite (upper) and schematic picture of cosmological magnetic fields generated from density fluctuations discussed here. Red (blue) regions are hot (cold) spots with a range of temperature $\sim 2.725 \text{ K} \pm 200\mu\text{K}$. The magnetic field vectors are shown together with the map. Strong magnetic fields are generated by currents where the gradient of density perturbation in photons is large.



Conclusions

- The Standard Model of Cosmology allows an almost perfect fit of many independent observations,
- but it relies on the existence of a few ingredients, like dark matter, dark energy today and vacuum energy during inflation whose nature and properties are largely unknown